EFFECT OF PORE SIZE DISTRIBUTION ON MULTIPHASE EQUILI BRIUM OF FLUIDS CONFINED IN POROUS MEDIA

A Thesis

by

ABDULHAQQ AMEEN IBRAHIM

Submitted to the Office of Graduate and Professional Studies of
Texas A&M University
in partial fulfillment of the requirements for the degree of

MASTER OF SCIENCE

Chair of Committee,	Marcelo Castier
Co-Chair of Committee,	Nimir Elbashir
Committee Members,	Ibrahim Galal Hassan
Head of Department,	M. Nazmul Karim

August 2016

Major Subject: Chemical Engineering

ABSTRACT

It is a well-known fact that the thermophysical properties of confined fluids (intraparticle) can be significantly different from those of bulk phases (interparticle). Such difference becomes more pronounced as the pore size decreases. The effect of confinement on the phase behavior of fluids is important for many applications, such as in adsorptive separations, extraction of shale oil and gas, and heterogeneous catalytic systems. The characterization of the porous solid material is of great relevance because the interactions of the solid with the molecules of the fluid play a major role in any modeling of confined fluid behavior. However, many solids are heterogeneous, in the sense that they have complex network structures, and pores of different sizes and of different chemical affinity with respect to the adsorbed molecules. Their effect on the properties of fluids entrapped in the porous space is not well captured by many models. One of the most important pieces of information to characterize solids is their pore size distribution, which is an intrinsic property of the material.

This thesis presents a method to account for the effect of pore size distributions on the phase behavior of fluids confined in porous media. Multiphase equilibrium calculations of confined fluids in solid adsorbents were carried out using the Peng-Robinson equation of state extended to confined fluids, while different pore size distributions of solid adsorbents were considered. The results obtained from the fitting of pure-component adsorption data revealed that the model correlations for fluids adsorbed in bipore solids were better when pore size heterogeneity was considered in the

formulation, as opposed to the assuming a homogeneous solid. Adsorption of n-hexane on MCM-48 solids with multiple pore size distributions was simulated as a model system, showing a trend of increasing accuracy of adsorption data fitting as the number of pore sizes increases. The sensitivity of the model to adsorption temperature was established by a few examples, suggesting that the model agreement with experimental data is better at higher temperatures.

DEDICATION

I dedicate this work to my beloved wife, Maryam Abeke and my son, Abdurrahman Akanbi. My special prayers to my late parents, may Allah have mercy on them as they took care of me when I was young.

ACKNOWLEDGEMENTS

I would like to use this opportunity to appreciate my committee chair, Dr. Marcelo Castier, and my committee co-chair, Dr. Nimir Elbashir, for their guidance, support and encouragement throughout the course of my study and this research work. My gratitude also goes to Dr. Ibrahim Galal Hassan, my committee member, for his constructive input. Words are not enough to express my appreciation to you all. Without your immense contributions and supports, this work would not have been a successful one.

I thank my friends, colleagues and the entire staff and faculty members of Chemical Engineering department for making my stay at Texas A&M University at Qatar a marvelous and indelible experience. My special thanks to Mr. Saad Intikhab, Mr. Sufiyan Mohammad Challiwala and Engr. Kabir Abdulyekeen. You are wonderful.

My profound appreciation goes to my brothers and sisters for their kind supports and words of encouragement throughout my master's program. I really appreciate you all.

This thesis was made possible by NPRP grant number 5-344-2-129 from the Qatar National Research Fund (a member of the Qatar Foundation). The statements made herein are solely the responsibility of the author.

NOMENCLATURE

Roman letters

A	Helmholtz free energy
a_p	Confinement modified energy parameter
b_p	Confinement modified volume parameter
E_{conf}	Configurational energy
f_{obj}	Objective function
f_k , f_k^{bulk}	Fugacities of the confined fluid and bulk phase fluid respectively.
F_p	Fraction of the fluid molecules in the confined space subjected to the attractive field of the pore walls.
i, j	Components indices notations
k	Boltzmann constant
$n_{\exp}$	Number of experimental data points
NC	Index denotes the number of fluid components of mixture
N_c	Total number of molecules
N_{av}	Avogadro's number
P_k^{bulk}	Specified bulk phase pressure at point k of the experimental data
P	Pressure
q_k	Adsorbed molar amount at point k of the experimental data
q	Internal partition function of one molecule

Q	Canonical partition function
R	Ideal gas constant
r_p	Pore radius
T	Absolute temperature
v_k	Molar volume of fluid confined inside the pore
v_k^L , v_k^V	Liquid-like and vapor-like molar volumes inside the pores at point k of the experimental data
V	Total volume
V_f	Free volume
v	Molar volume of the fluid
x	Mole fraction

Greek letters

α	Vaporized fraction within the pores
δ_p	Square well width molecule-wall interaction potential
ε	Molecule-molecule interaction energy parameter
ε_p	Molecule-wall interaction energy parameter
θ_i	Geometric term
λ	De Broglie wavelength
μ_i	Chemical potential
ρ_{max}	Confinement-modified molecular packing density
σ_{ij}	Average molecular diameter for components *i* and *j*

TABLE OF CONTENTS

Page

ABSTRACT ii

DEDICATION iv

ACKNOWLEDGEMENTS v

NOMENCLATURE vi

TABLE OF CONTENTS viii

LIST OF FIGURES x

LIST OF TABLES xii

1. INTRODUCTION 1

   1.1 Research problem 3
   1.2 Research aim and objectives 3
   1.3 Organization of this thesis 4

2. LITERATURE REVIEW 5

   2.1 Equation of state for confined fluids 5
   2.2 Development of equation of state for confined fluids 11
   2.3 Adsorption process in porous structures 14
   2.4 Equilibrium condition of adsorbed fluids in confinement 16
   2.5 Pore size distribution 20
   2.6 Abilities and prospects of alumina support with bimodal pore in FTS 23

3. FORMULATION AND SOLUTION METHODS 26

   3.1 Research procedures 30
   3.2 Equilibrium calculations and parameter fitting 31

4. RESULTS AND DISCUSSION 34

   4.1 Program validation 34
   4.2 Illustration of pore size distribution 37
   4.3 Effect of pore size distribution on adsorption isotherm 38

4.3.1 Adsorption of pure components on MCM-48 39
4.3.2 Adsorption data fitting for multiple pore size distribution 49
4.4 Relationship between bulk phase density and bulk pressure 54
4.5 Temperature dependence of the model 56

5. CONCLUSION AND FUTURE WORK 60

5.1 Conclusions 60
5.2 Future work 62
5.3 Program availability 63

REFERENCES 64

APPENDIX A 73

LIST OF FIGURES

Page

Figure 1: Schematic illustration of the first and second layer of adsorption; the multi-layers adsorption approaches a liquid-like phase configuration.. 16

Figure 2: Nitrogen adsorption isotherm on the SBA-15 silica at 77.4 K. 17

Figure 3: Comparison of experimental isotherms of N_2 at 77.4 K on MCM-41 type material and NLDFT model.. 19

Figure 4: Schematic cross-sectional view of a porous solid. 21

Figure 5: Flow chart of the multiphase equilibrium calculation algorithm 33

Figure 6: Parameter estimation for methane on activated alumina at 323.15 K using Excel XSEOS package and FORTRAN program 35

Figure 7: Parameter estimation for propane on activated alumina at 313.15 K using Excel XSEOS package and FORTRAN program. 36

Figure 8: Parameter estimation for butane on activated alumina at 313.15 K using Excel XSEOS package and FORTRAN program 36

Figure 9: Pore size distribution for unimodal conventional alumina support (Alumina-C) 37

Figure 10: Pore size distribution for bimodal alumina support (Alumina-H) 38

Figure 11: Adsorption data fitting for acetone on unipore MCM-48 at 323.15 K 41

Figure 12: Adsorption data fitting for acetone on bipore MCM-48 at 323.15 K 42

Figure 13: Adsorption data fitting for methanol on unipore MCM-48 at 323.15 K 43

Figure 14: Adsorption data fitting for methanol on bipore MCM-48 at 323.15 K 44

Figure 15: Adsorption data fitting for benzene on unipore MCM-48 at 323.15 K 45

Figure 16: Adsorption data fitting for benzene on bipore MCM-48 at 323.15 K 45

Figure 17: Adsorption data fitting for cyclohexane on unipore MCM-48 at 323.15 K 46

Figure 18: Adsorption data fitting for hexane on unipore MCM-48 at 323.15 K. 47

Figure 19: Adsorption data fitting for cyclohexane on bipore MCM-48 at 323.15 K .. 48

Figure 20: Adsorption data fitting for hexane on bipore MCM-48 at 323.15 K 48

Figure 21: Adsorption data fitting for hexane on tripore MCM-48 at 323.15 K 51

Figure 22: Adsorption data fitting for hexane on quadpore MCM-48 at 323.15 K 51

Figure 23: NLDFT pore size distribution curve from argon sorption isotherm on MCM-48 silica at 87 K 52

Figure 24: Adsorption data fitting for cyclohexane on tripore MCM-48 silica at 323.15 K 53

Figure 25: Plot of bulk pressure against density of methanol adsorption on unipore and bipore MCM-48 at 323.15 K. 54

Figure 26: Plot of bulk pressure against density of benzene adsorption on unipore and bipore MCM-48 at 323.15 K. 55

Figure 27: Plot of bulk pressure against density of hexane adsorption on unipore and bipore MCM-48 at 323.15 K. 56

Figure 28: Adsorption data fitting for methane on bipore ZSM-5 at 276.95 K 58

Figure 29: Adsorption data fitting for methane on bipore ZSM-5 at 307.95 K 58

Figure 30: Adsorption data fitting for methane on bipore ZSM-5 at 352.75 K 59

LIST OF TABLES

Page

Table 1: FORTRAN program validation with Excel XSEOS package 35

Table 2: Adsorption data fitting for pure polar and non-polar component on MCM-48 results. 40

Table 3: Pure hexane adsorption on multipore MCM-48 results 49

Table 4: Pure cyclohexane adsorption fitting on tripore MCM-48 silica 53

Table 5: Pure methane adsorption on ZSM–5 results 57

1. INTRODUCTION

In the study of thermodynamics, the phase behavior of fluids can be affected by various parameters and conditions to which the fluid is subjected. It has been observed over a long period of time that many physical properties of fluid confined in porous structures (intraparticle) as well as its phase equilibrium change significantly from the unconfined or bulk state (interparticle). This effect of confinement on fluid properties becomes more pronounced as the sizes of the pores decrease. Phase transitions such as pore condensation may occur as a result of the strong interaction between the solid wall of the pores and the fluid molecules in the confined space with different temperatures and pressures from those in the bulk [1].

This effect is often encountered in many applications such as in separation processes involving adsorption, extraction of oil and gas entrapped in porous reservoir rocks, and heterogeneous catalytic reactive systems, as in the case of Fischer-Tropsch synthesis (FTS). A clear understanding of this phenomenon is therefore important to correlate and predict this effect accurately.

Many attempts have been made to develop models based on existing cubic equations of states (EOS) that can predict the thermodynamic properties of pure fluids and mixtures at the microscopic scale (inside the pores) and macroscopic scale (outside the pore). These models seem to be appealing to many chemical and oil and gas industries due to their ease of computation and sufficiently accurate prediction of thermodynamic properties for chemical process design. Travalloni *et al*. [2] extended the Peng Robinson

(PR) EOS to confined fluids by considering the effect of molecule–wall interactions, pore size and shape. The model is capable of predicting the phase behavior of fluid in the bulk and confined space as well as simultaneously accounting for the effect of multiple pore types of different sizes (heterogeneous adsorbents) and interaction energies.

A typical case is the Fischer-Tropsch catalytic system, as there may be mass transfer limitations of the reactants flowing from the bulk phase inside the reactor bed (macro-scale) into the catalyst pores (micro-scale) where active sites are located. Likewise, there may be limitations to the diffusion of the product mixtures from the pore to the bulk phase inside the reactor, especially in the fixed bed reactors. This is a result of heavy hydrocarbons condensing inside the catalyst pores as the reaction proceeds at high densities within the pores, thereby limiting the access of the reactants to the active sites. Furthermore, the choice of the reaction media, such as the gas phase or liquid phase reaction, plays a major role on the FTS product distribution and influences fluid transport in and out of the catalyst pores [3]. In order to maximize the utilization of the active sites, it is necessary to study the phase behavior of the fluid mixture in the confined space inside the pores of the catalyst. This motivated the introduction of supercritical fluids in FTS as thought to reduce the chances of capillary condensation and mass transfer limitations by providing a homogeneous phase for the syngas and products mixtures [4]. However, the scarcity of experimental data on the behavior of confined FTS fluids limits the ability to use the modeling approach developed in this thesis.

1.1 Research problem

As described in the previous section, modelling the phase behavior of fluids confined inside porous materials and in the bulk of a system will allow better understanding and control of the process systems in many applications. However, many adsorption models commonly used do not explicitly account for the effect of pore size distributions and shapes within the cavities of the adsorbent. Pore size distribution is an intrinsic property of porous materials, which can influence the thermophysical properties of fluids entrapped in them. Hence, it is quite important to study the effect of pore size distribution on phase behavior of fluids in confined space.

Warrag [5] studied the phase behavior of confined fluids using the extended PR EOS for confined fluids considering one pore type (unipore size distribution). The number of phases existing in the bulk and confined space at different operating pressures as well as the possibilities of pore condensation were investigated with emphasis on Fischer-Tropsch catalytic systems

In contrast to Warrag's work [5], this research will employ the PR EOS for confined fluids to investigate the effect of multiple simultaneous pore sizes on the phase behavior of fluids confined in porous media. This is a more realistic representation of porous solids. Therefore, this work will address the problem of accounting for pore size distributions in the calculation of phase equilibrium with an EOS.

1.2 Research aim and objectives

The aim of this work is to investigate the effect of pore size distribution on the phase behavior of fluids in porous structures. Discrete number of pores were used to

represent the pore size distribution for simplicity of approach. In order to establish the relationships between pore size distributions and phase behavior of fluids especially in the confined space, the following objectives must be achieved:

1. To characterize the nature of phases existing in the bulk (outside the pores) and within the porous material, whose pore sizes are typically in the range from 2 to 50 nm.
2. To verify the occurrence of pore condensation in materials with multiple pore sizes.
3. To correlate and predict fluid phase behavior within porous solids with representative bipore size distributions.

1.3 Organization of this thesis

This thesis has five chapters. Subsequent to this introductory chapter, chapter 2 presents a literature review that focuses on equations of state for confined fluids and on the properties of fluids confined in materials with multiple pore sizes.

Chapter 3 provides details about the PR EOS extended to fluids within cylindrical pores used in this work and the algorithms used for phase equilibrium calculations and parameter fitting.

Chapter 4 presents the results and discussion of this work. The first of them validates the FORTRAN code utilized in this work against an independent implementation of the same model. The other results of this chapter are for fluids within materials with multiple pore sizes.

The final chapter outlines the conclusions drawn from this research and presents proposals for future investigation.

2. LITERATURE REVIEW

2.1 Equation of state for confined fluids

Many attempts have been made to develop confined fluid models. Approaches such as molecular simulations and density functional theory tend to give detailed descriptions of confined fluid local properties. Their applicability is limited to more complex problems such as the spatial distribution of a fluid mixture in a heterogeneous porous matrix because of high computational effort [6]. Examples of these kinds of investigation include the work of Coasne *et al.* [7], who studied the effect of confinement on the adsorption, capillary condensation, and freezing/melting of fluids in nanopores using Grand Canonical Monte Carlo simulations. It was found that the adsorption of benzene at 298 K in a cylindrical silica nanopore of a diameter 3.6 nm involves a transition from a partially filled pore to a completely filled pore configuration.

Another example, among many others, is the work of Kotdawala *et al.* [8] who investigated the effect of nano-confinement on the thermodynamic properties of fluids using density functional theory with mean-field approximation in narrow slit-pores. A model for predicting the adsorption of binary mixtures of nonpolar molecules, as well as polar molecules was proposed and the relative contributions of fluid-wall and fluid-fluid interactions were studied from the simulated results. Neimark and Ravikovitch [9] studied the pore condensation/evaporation of Nitrogen and Argon in the mesoporous molecular sieves (MMS) with cylindrical channels using the non-local density functional theory (NLDFT). The model employed Lennard-Jones potentials and accounted for the

interactions potentials between the molecules of the fluid as well as the solid-fluid. The adsorption/desorption isotherm predictions were in good agreement with the experimental data, however with a significant deviation in pores smaller than 5 nm. The method was also developed for pore size distribution calculations.

Another approach is modeling the behavior of confined fluids using analytical EOS, with parameters fitted to experimental data. This approach gives less detailed description of fluid behavior, but offers results which are sufficiently accurate for chemical process design [6]. It is much faster from the computational viewpoint than the techniques mentioned earlier.

Some of the previous work on the development of confined fluid model based on equations of state approach is reviewed here. Schoen and Diestler [10] developed a model for a simple fluid confined in a slit-pore based on thermodynamic perturbation theory. The temperature and density dependence of the resulting model was similar to that of the bulk fluid of van der Waals equation of state. A reference hard sphere fluid of uniform density was assumed and attractive interactions were added as correction. The model was able to predict pore condensation over a range of densities. However, the performance of the model near the critical point of the bulk fluid was unsatisfactory. Giaya and Thompson [11] developed a model for water-like fluids confined in cylindrical micropores using perturbation theory as an extension to the Schoen and Diestler [10] model. The model accounted for fluid–fluid, fluid–wall both as the pairwise sum of Lennard-Jones potentials, and hydrogen bonding interactions. Good predictive results for water adsorption were obtained with this model.

Zhu *et al.* [12] proposed an equation of state for films adsorbed in cylindrical mesopores, which considered the attractive interactions between the adsorbed molecules and solid adsorbent, the surface tension, and the curvature of gas/adsorbed phase interface. The model was based on thermodynamic interface theory and described the adsorption of nitrogen on MCM-41 samples with different pore sizes. The model was able to predict pore condensation and established a quantitative relationship between the pore radius and the condensation pressure. Derouane [13] also developed a model for fluids confined in microporous solids by proposing a modification to the van der Waals equation of state to represent the attractive term better. The physical states of adsorbed molecules in microporous materials were determined below pore saturation.

Zarragoicoechea and Kuz [14] proposed a model for a confined fluid in a nanopore from the generalized van der Waals equation of state and considered the tensorial nature of pore pressure. The formulation was based on classical thermodynamics with assumption of a square section nanopore of infinite length and neglected the attractive molecule–wall interaction effect. The model predicted vapor-liquid equilibrium, pore condensation, and shift of the critical parameters, which were in good agreement with the results obtained from numerical simulations. Also, the results of critical temperatures were consistent with experiment data.

Travalloni *et al.* [6] proposed an extended form of the van der Waals EOS for confined fluids in cylindrical pores. The square-well potential was used to account for the molecule-molecule as well as the molecule-wall interactions in the model. This model has two adjustable parameters that characterize the molecule-wall interactions and makes it

suitable for predicting fluid behavior in the confined space as well as in the bulk. Travalloni *et al.* [2] further used this approach to extend the PR EOS to model fluids confined in porous media.

Useful thoughts and directions from previous work led to better understanding of the phase behavior of a variety of compounds in confinement and have been used to develop thermodynamic models for different applications. Recently, Tan *et al.* [1] described the phase equilibrium of fluids confined in nanoporous materials using the perturbed-chain statistical associating fluid theory (PC-SAFT) EOS in conjunction with the Young–Laplace equation. The model considered the pore geometry, surface tension, and accounted for solid-fluid interactions using the contact angle of the fluid surface to the solid wall. The interaction between the pore walls and the fluid is represented by a parameter that is a function of pore size and adjustable to the experimental data. The PC-SAFT/Laplace model could be used to predict the phase transition during pore condensation. The multilayer adsorption preceding pore condensation was not considered in this model since the phase equilibrium at the point of capillary condensation was the sole interest as required in shale gas and tight oil applications.

Akand *et al.* [15] developed a modified van der Waal EOS to describe the phase behavior of fluids confined in nanopores. An inert pore wall was assumed and Maxwell's equal area rule was applied to investigate phase change due to pore confinement without any additional scaling of model parameters. The model was compared with the classical PR EOS. The modified van der Waals EOS demonstrated critical shift in pressure and temperature, and predicted capillary condensation. These results were in good agreement

with experimental data and molecular simulation results, while the PR EOS predicted a dense supercritical state as the effect of pore confinement.

Jamili *et al.* [16], more recently, developed a model based on coupled Simplified Local-Density theory and Modified Peng-Robinson EOS (SLD-PR model) to predict the fluid density profiles of fluids inside nanoporous solids, from which adsorption isotherms of pure hydrocarbons and mixtures are generated. The model predicted fluid distributions across the slit pores showing the occurrence of multi-layer adsorption near the pore walls with the heaviest component next to the pore wall. The results compared accurately well with those obtained from experimental data and molecular simulations in the literature. However, this model only considered a smooth and ideal slit-pore type for simplicity, which is far from reality. Dong *et al.* [17] used a similar approach of coupled model, and the phase behavior of pure fluids and mixtures confined in cylindrical pores were predicted using the PR EOS coupled with an improved Young-Laplace equation and adsorption theory. It was observed that the narrower the pore size the more is the deviation between the actual value of vapor-liquid equilibrium constant (K-value) and the predicted value.

The study of phase behavior of fluids confined in the porous media has found a wide range of applications in organic rich shale reservoirs, as they have become an important energy resource in the world. It gives better understanding of the fluids properties and flow mechanism of the confined fluids within the porous cavity of the rock. Due to the demand for an improved techniques of oil and gas extraction from shale reservoir, many attempts have been targeted towards predicting the thermodynamic

equilibrium conditions of multi-component hydrocarbons entrapped in shale porous structures. Some of the work done in this line are reviewed next.

Yinghui *et al.* [18] formulated a novel technique to characterize the capillary pressure and considered the effect of pore size distribution on the phase behavior and flow characteristics of confined fluids in unconventional reservoir. An Optimized Simplified Local Density (OSLD) PR EOS Model with fluid-fluid and fluid-solid interactions terms was developed to incorporate adsorption behavior for CO_2 capture, utilization, and storage in the nanopores of shale formations. This enables the prediction of multi-component interactions over a range of reservoir pressures.

Dhanapal *et al.* [19] also demonstrated the effect of pore confinement in conjunction with pore size distribution and pore networks on phase behavior of methane in the porous shale rock. The extended PR EOS for confined fluids developed Travalloni *et al.* [2] was adopted due to the wide spread usage of PR EOS in the oil and gas industries. It was extended to evaluate the effective pores size. A satisfactory result was obtained from the model when the smallest pores accounted for a small percentage of the entire pore volume. Otherwise, prediction of the multiphase equilibrium conditions becomes difficult.

Ma *et al.* [20] modified the van der Waals EOS to investigate the phase behavior and properties of hydrocarbon fluids confined in tight shale formations by considering the molecular interaction effects of fluid-fluid and fluid-pore wall. The molecule-pore wall interaction were estimated from molecular simulation results and the methodology could be extended to other cubic EOS. The effects of pore proximity on phase behavior of fluids

were determined corresponding to the model sensitivity. For the confined fluid mixture under consideration, it was observed that the two phase region of the fluid mixture become smaller when the capillary size decreases. The model revealed that the bubble point and dew point pressures of the confined fluids were much higher than the corresponding bulk phase values, and more of heavier hydrocarbon molecules evaporate as confinement increases.

In this work, the extended PR equation of state for confined fluids [2] was employed for equilibrium calculation of thermosphysical properties of fluids in porous structures with representative pore size distributions, for its simplicity and sufficiently accurate predictions of fluid behavior in the bulk and in the pore.

2.2 Development of equation of state for confined fluids

Travalloni *et al.* [6] successfully developed a confined fluid model based on the generalized van der Waals theory. The model is an extension of van der Waal cubic equation of state which is able to predict the behavior of pure fluids as well as mixtures confined within the cavities of porous materials.

The thermodynamic relations, as stated by Hill [21], for the canonical partition function (Q) were used to obtain the confined fluid equation of state and the chemical potential (μ_i) of each component analytically.

$$P = kT\left(\frac{\partial \ln Q}{\partial V}\right)_{T,N_1,N_2,\ldots,N_{NC}} \tag{2.1}$$

$$\mu_i = -kT\left(\frac{\partial \ln Q}{\partial N_i}\right)_{T,V,N_{j\neq i}} \tag{2.2}$$

where P is the pressure, k is the Boltzmann constant, T is the absolute temperature, V is the total volume of the system, N_i is the number of molecules of the components i, and NC is the number of components of the mixture. The model development was started from the canonical partition function, which represents a window between statistical and classical thermodynamics because all thermodynamic properties of a fluids can be calculated from the canonical partition function [21], which is:

$$Q(T,V,N_1,N_2,...,N_{NC}) = \prod_{i=1}^{NC}\left(\frac{q_{\text{int},i}^{N_i}}{\lambda_i^{3N_i} N_i!}\right) V_f^N \quad \exp\left(\int_{\infty}^{T} \frac{E_{conf}}{kT^2} dT\right) \tag{2.3}$$

where $q_{int,i}$ is the internal partition function of one molecule of component i, λ_i is the de Broglie wavelength of component i, V_f is the free volume, E_{conf} is the configurational energy, and other symbols remain the same as defined earlier.

The following assumptions were made to develop expressions for the free volume and configurational energy in order to account for the molecule-wall interactions in the confined space; spherical fluid molecules with square-well interaction potentials and the adsorbent pores are cylindrical [6]. For mixtures, the values of V_f and E_{conf} are given by the following expressions, respectively:

$$V_f = V - \sum_{i=1}^{NC} \frac{N_i}{\rho_{\max,i}} \tag{2.4}$$

$$E_{conf} = -\sum_{i=1}^{NC}\sum_{j=1}^{NC}\left(\frac{N_j}{2} N_{C,ij}\varepsilon_{ij}\right) - \sum_{i=i}^{NC}\left(N_i F_{p,i}\varepsilon_{p,i}\right) \tag{2.5}$$

where $\rho_{\max,i}$ is the molecular density of pure component *i* in a packed structure, $N_{C,ij}$ is the number of molecule of component *i* around a central molecule of component *j*, ε is the molecule-molecule interaction energy parameter, $\varepsilon_{p,i}$ is the molecule-wall interaction energy parameter for component *i*, and $F_{p,i}$ is the fraction of the fluid molecules in the confined space of component *i* that interact with the pore walls [2, 6].

The expression below is the extended PR equation of state for confined fluids as proposed by Travalloni *et al.* [2];

$$P = \frac{RT}{v - b_p} - \frac{a_p(T)}{v\left(v + b_p\right) + b_p\left(v - b_p\right)} - \sum_{i=1}^{NC}\left(x_i\theta_i \frac{x_i b_{p,i}}{v^2}\left(1 - \frac{x_i b_{p,i}}{v}\right)^{\theta-1}\left(1 - F_{pa}\right)\times\left(RT\left(1 - \exp\left(-\frac{N_{av}\varepsilon_{p,i}}{RT}\right)\right) - N_{av}\varepsilon_p \right)\right) \tag{2.6}$$

where v is the molar volume of the fluid, θ is the geometric term, *x* is the molar fraction, *R* is the universal gas constant and N_{av} is the Avogadro number. a_p and b_p are the confinement modified energy and volume parameters for fluid mixtures, respectively. The expressions for a_p and b_p depend on the extent of confinement and are given by the following expressions:

$$a_p = \sum_{i=1}^{NC}\sum_{j=1}^{NC}\left(x_i x_j \sqrt{a_i a_j}\left(1 - \frac{2}{5}\frac{\sigma_{ij}}{r_p}\right)\right) \tag{2.7}$$

$$b_p = \sum_{i=1}^{NC} x_i\left(\frac{N_{av}}{\rho_{\max,i}}\right) \tag{2.8}$$

where r_p is the pore radius and σ_{ij} is the average molecular diameter for components *i* and *j*. Additional information about the model is available in Appendix A of this thesis.

The detailed derivations of the extended PR EOS for confined fluids and the formulas of all auxiliary terms can be found in Travalloni *et al.* [2, 6]. This model is valid for confined fluid prediction as well as bulk fluid, as the pore radius become infinitely large, the confinement effect vanishes and the EOS reduces to the original form. The size and energy of interaction are the two adjustable parameters of this model and they depend on the pair solid-molecule of the fluid. They can be obtained by fitting to the experimental adsorption data for pure fluids.

2.3 Adsorption process in porous structures

Adsorption is a phenomenon that takes place next to solid-fluid interfaces and is governed by specific interactions between the atoms at the solid surface and the molecules approaching the surface from the gas (or the liquid) phase [22]. Adsorption can be sub-divided into Physisorption (physical adsorption) and Chemisorption (chemical adsorption).

Physisorption is often referred to as van der Waals adsorption due to the van der Waals interaction between gas molecules and solid surface which is the major driving force for adsorption as the intrinsic binding energy. The van der Waals interaction energy in physisorption is usually not more than 15 kJ/mole and the adsorption heat is about 20~40 kJ/mole, which account for its very weak attraction [23]. Physisorption can occur spontaneously as molecules strike the solid surface because it does not require activation energy. The process is fully reversible and equilibrium is established very rapidly unless diffusion through small pores limits the adsorption rate. The equilibrium may be metastable in the case of systems showing hysteresis [24].

Chemisorption on the other hand is an irreversible adsorption process whereby the adsorbed molecules are more localized on the surface when compared to physical adsorption due to the formation of a chemical bond between an adsorbate molecule and a specific site on the surface the adsorbent. Valence forces of the same kind as those operating in the formation of chemical compounds are involved [25]. According to Lowell *et al.* [26], chemisorption is characterized mainly by large interaction potentials and usually associated with an activation energy, which leads to high heats of adsorption often approaching the value of chemical bonds.

By definition, the fractional coverage of the adsorbed fluids, at a given equilibrium pressure *P*, is the ratio of surface sites occupied by the adsorbed fluids *Ns* over the total available adsorption sites *N*. The first layer of adsorbed phase termed monolayer adsorption is due to either physisorption or chemisorption, or both, according to the nature of the forces governing the solid-fluids interactions. Conversely, any additional layer, multilayer adsorption is as a result of physical forces, similar to the forces that lead to the non-ideal behavior of gases and eventually to the condensation of the fluids. As such, subsequent layers are expected to approach a liquid-like phase configuration [22]. Figure 1 describes the formation of adsorption layers as it approaches liquid-like phase configuration.

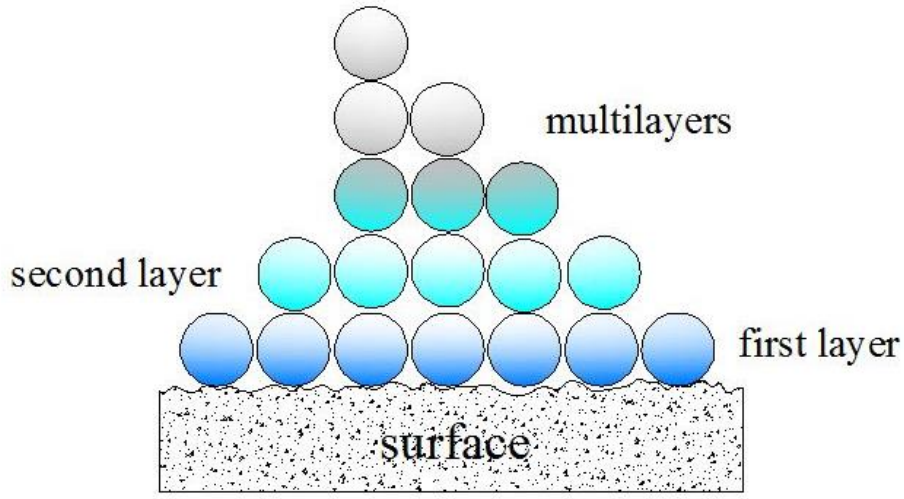

Figure 1: Schematic illustration of the first and second layer of adsorption; the multi-layers adsorption approaches a liquid-like phase configuration. Adapted from Bolis, 2013 [22].

The fraction of monolayer coverage, θ can be represented by the following expression:

$$\theta = \frac{V}{V_{\max}} \tag{2.9}$$

where V is the gas volume adsorbed per unit weight of solid at pressure, P and V_{max} is the maximum monolayer volumetric capacity per unit weight of solid.

Also, the multilayer adsorption leading to pore filling can be defined as the volume of gas physically adsorbed relative to that volume adsorbed at multilayer saturation [27].

2.4 Equilibrium condition of adsorbed fluids in confinement

Adsorption is often used to describe the condensation of gases on surfaces or inside porous materials. Capillary condensation is the process by which the pore spaces become filled with condensed liquid as a result of continuous multilayer adsorption of the vapor

phase molecules in a porous medium. For a pure fluid, the vapor condenses inside the capillary at a pressure below its saturation vapor pressure *P* at a given temperature due to an increasing van der Waals force of attraction between vapor phase molecules inside the porous structure. The condensation pressure depends on the pore shape, size and on the energy of interaction between the fluid and pore wall [9]. An equilibrium below the saturation vapor pressure is set at the liquid-vapor interface through the formation of meniscus once condensation has occurred. Figure 2 represents a typical adsorption isotherm of nitrogen on SBA-15 silica at 77.4 K. The hysteresis loop, capillary condensation, and evaporation in adsorption and desorption branches, respectively, are indicated in Figure 2.

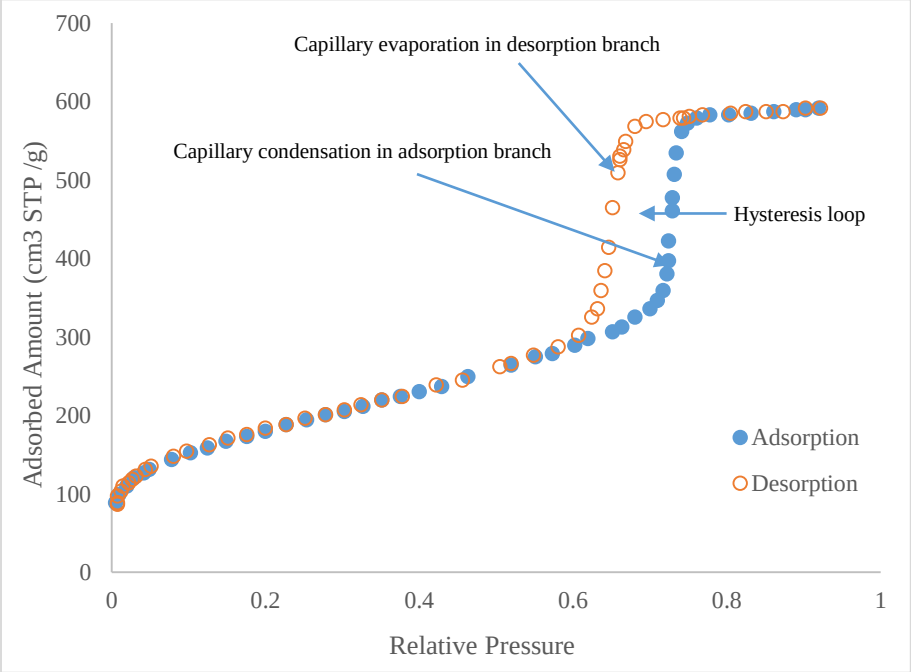

Figure 2: Nitrogen adsorption isotherm on the SBA-15 silica at 77.4 K. Adapted from Grosman and Ortega, 2005 [28]

In most of adsorption/desorption processes, the path through which capillary condensation occurs differs from the one followed during desorption, leading to hysteresis in the adsorption system. The pressure at which capillary condensation takes place upon adsorption is often larger than that of capillary evaporation during desorption. Consequently, the pore size distribution calculated from adsorption and desorption differ significantly [26]. It has been observed that different mechanisms of condensation and evaporation could cause adsorption/desorption hyterisis and also depends upon the shape and size representing the geometry of the pores [29]. Recently, methods of statistical mechanics, molecular dynamics and density functional theory have been used to develop quantitative analysis of capillary condensation in porous structures [9].

It has become clear that the hysteresis results from the metastable state of fluids in confined phase for unconnected cylindrical pores. Thommes *et al.* and Neimark and Ravikovitch [9, 30] applied the non-local density functional theory (NLDFT) method to the adsorption branch of the isotherm, which accounted for the effect of delayed vapor-liquid transition during capillary condensation in pores of different sizes and shapes. Figure 3 shows a comparison between the experimental isotherm of nitrogen adsorbed on MCM-41 at 77.4 K and the NLDFT model prediction.

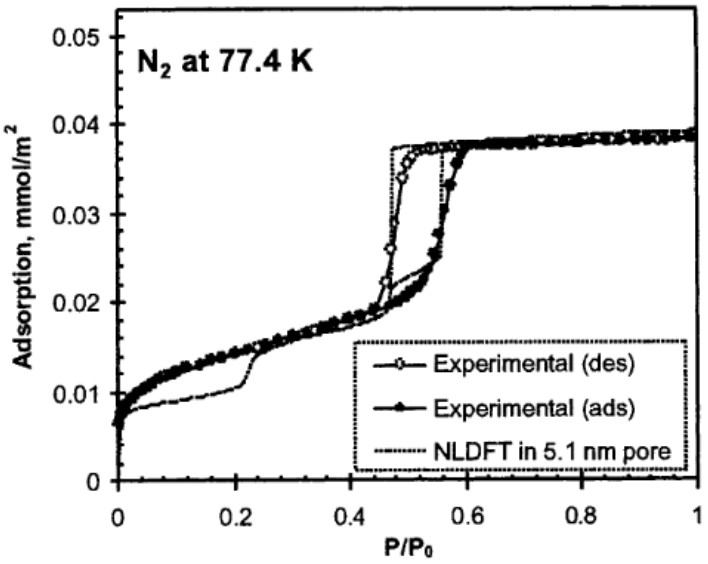

Figure 3: Comparison of experimental isotherms of N_2 at 77.4 K on MCM-41 type material and NLDFT model. Adapted from Thommes *et al.,* 2006 [30].

The NLDFT model quatitatively predicted main features of the experimental isotherm such as the total adsorbed amount, pressures of spontaneous pore condensation (adsorption) and evaporation (desorption). It was observed that the theoretical equilibrium transitions of the capillary condensation and evaporation correspond to the respective turning points of the experimental isotherm, which shows good agreement between the two. Neimark and Ravikovitch [9], however suggested that the stepwise pattern and vertical equilibrium transitions observed in the theoretical model were not present in the experimental isotherm. These may be due to the heterogeneity of the pore size and extent of the non-uniform pore channels [9].

This effect of delayed vapor-liquid transition during capillary condensation can be attributed to the existence of metastable adsorption films inside the pores [26, 9]. It was

predicted that, as adsorption proceeds, the vapor-like states above the equilibrium transition pressure are metastable and terminate at the limit of stability (vapor-like spinodal) for the metastable adsorbed films after which the fluid suddenly condenses into a liquid-like phase. On the other hand, the desorption branch remains metastable below the equilibrium transition pressure until it reaches the liquid-like spinodal which corresponds to the limit of stabilty. At this point, spontaneous evaporation will occur [9, 30].

For a uniform open-ended cylindrical pore, there is no metastable condition on the desorption branch and hence, associated with the equilibrium vapor-liquid transition, as opposed to the adsorption branch [30].

2.5 Pore size distribution

Porous solids are solids with cavities, channels or interstices, which are deeper than they are wide. They can be characterized by their porosity and pore size distribution, the portion of the solid's volume that is not occupied by or isolated by solid material [22]. Chemical reactivity and physical interactions of solids with gases or liquids are often influenced by porosity. Physical characteristics of porous solids like as surface area, density and thermal strength are function of its porosity and the structure of the pore [31]. It is therefore very important to control the porosity of solids to well-structured pore networks for industrial applications. Various applications of porous materials such as heterogeneous catalysis, structural materials, adsorbents, molecular and membranes separation have attracted great interest to study porous structures and its control at

different levels [32]. Figure 4 depicts the cross-sectional view of a porous soild and its various features.

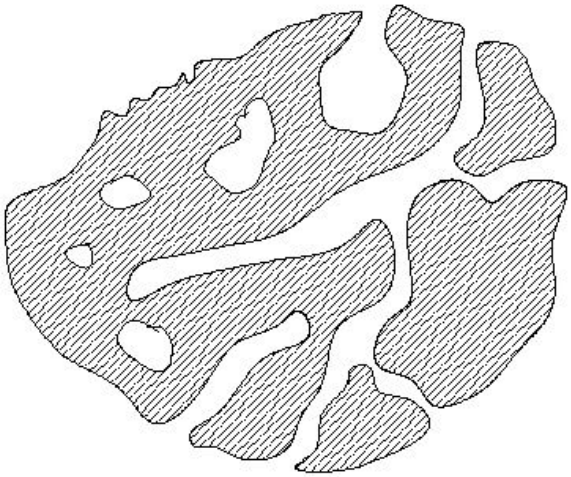

Figure 4: Schematic cross-sectional view of a porous solid. Adapted from Rouquerol *et al.*, 1994 [33]

Rouquerol *et al.* [33] gave the quantitative description of a porous solid as depicted in Figure 4. Pores can be classified based on their availability to the bulk fluid and their shapes. Closed pores are totally isolated from their surroundings and are not accessible to fluid flow or gas adsorption. However, open pores of different shapes such as cylindrical, ink-bottle and slit shaped are readily available to external fluids. Macroscopic properties of materials such as thermal conductivity, bulk density and mechanical strength are influenced by these pores.

Pore size distribution is the distribution of pore volume or area with respect to pore size. i.e. $\frac{dV_p}{dr_p}$ or $\frac{dA_p}{dr_p}$ as a function of r_p. According to the IUPAC classification, pores are characterized based on their sizes [22, 24]; pore diameters of microporous solids are less than 2 nm, of mesoporous solids lie between 2 nm and 50 nm and solids with pore diameters greater than 50 nm are categorized as macroporous solids.

In the recent times, methods for preparing well-structured inorganic porous solids with different size orientations and distributions have been developed to suit particular applications of interest. Methods such as physical templating have been used to prepare large mesopores or macroporous materials [34], as well as chemical templating by primary particle seeding and post-hydrothermal treatment, which allows independent control of the smaller and larger mesopore sizes [35].

Micropores and mesopores can selectively adsorb molecules, as reported by Pauly *et al.* [36], and the combination of well-connected small and large mesopores can reduce transport limitations in heterogeneous catalysis applications, leading to better activities and enhanced selectivity control. Levenspiel [37] also demonstrated that bimodal catalysts can significantly enhance diffusion efficiency and provide wider supported surface area.

Different methods have been proposed to calculate pore size distribution from adsorption data. One of the most common method is the one proposed by Barett-Joyner-Halenda (BJH) [38], under the assumption that the equilibrium between the gas phase and the adsorbed phase is determined based on physical adsorption on the pore walls and capillary condensation in the inner capillary volume in the desorption branch. Dollimore and Heal [39] suggested an improvement to the calculation of pore size distribution due

to the difficulty of calculations in the previous methods. Multilayers of adsorbed molecules remain on the inner wall of the pores which thins out continuously as desorption proceeds even when there is no condensed liquid in the pores. Thus, the actual radius of the pore is more than the meniscus radius of the capillary condensate. These approaches are presented in details elsewhere [29, 30].

Variation of pore shapes and sizes of porous materials can play a major role in many applications, as is heterogeneous catalytic systems such as FTS.

2.6 Abilities and prospects of alumina support with bimodal pore in FTS

Fischer-Tropsch synthesis is the catalytic conversion of syngas (carbon monoxide (CO) and hydrogen (H_2)) derived from biomass, coal or natural gas into ultra-clean fuels and petrochemical substituents [40]. It is an important basis of gas-to-liquids (GTL), coal-to-liquid (CTL) and biomass-to-liquid (BTL) technologies which enable the production of chemicals and transportation fuels from sources other than crude oil. The process was discovered by Franz Fischer and Hans Tropsch in 1923 [41]. In it, hydrocarbons mixture of wide range of carbon numbers are synthesized by converting CO and H_2 mixture using iron catalyst. There are three major configuration of FTS reactors widely used commercially: fixed bed reactor, slurry bubble column, and fluidized bed reactor. The overall FTS over a typical cobalt-based catalyst can be represented as follows:

$$nCO + (2n+1)H_2 \rightarrow C_nH_{2n+2} + nH_2O \qquad (2.10)$$

It has been established that the choice of catalyst is of high importance in FTS and has significant effect on the product distribution. Catalyst performance such as activity,

product selectivity, and lifetime are the key contributors to FTS catalytic system efficiency [40].

The choice of support has also been reported to play a major role in FTS activity in terms of the active site loading, dispersion, reduction, and active site-support interaction [31, 42]. Alumina is one of the most commonly used catalyst support for commercial FTS catalysts due to its high thermal stability and mechanical resistance as well as large surface area [32, 33]. It was reported that the physical-chemical properties of alumina have strong influence on the catalytic performance of alumina supported cobalt catalysts [23, 33].

However, most of the conventional mesoporous alumina used commercially are unimodal in nature. Bimodal pore type alumina supports have been proven to be more effective and desirable for industrial applications. Tsubaki *et al.* [43] reported that cobalt catalyst supported on bimodal silica showed significantly increased activity in liquid-phase FTS.

According to the studies of Li *et al.* [44], different cobalt catalysts supported on nanostructured alumina for FTS were prepared and compared with commercial alumina. It was observed that alumina nanorods supported catalysts with bimodal pore size distribution showed the best cobalt dispersion after reduction and highest conversion of CO at steady state. The aforementioned catalysts showed higher stability coupled with lower methane selectivity.

Liu *et al.* [45] prepared different kinds of cobalt alumina support catalyst and evaluated FTS catalytic performance in a fixed bed reactor. They found that Cobalt-alumina supported catalyst with bimodal pore size distribution gave the largest specific

surface area, smallest cobalt particle size, highest CO conversion and lowest methane selectivity for FTS when compared with the conventional unimodal alumina supported catalysts, at the same conditions.

3. FORMULATION AND SOLUTION METHODS

The two adjustable parameters of the PR EOS extended to confined fluids, i.e., the characteristic energy parameter $\delta_{p,i}$ and characteristic size parameter $\varepsilon_{p,i,}$, were estimated by fitting the experimental adsorption data of pure components adsorbed on solid adsorbents. The pore size(s) corresponding to their specific pore volume depending on the pore size distribution of the solid were specified and an idealized cylindrical pore shape assumed. This task was carried out using a FORTRAN code that implements the thermodynamic model and the necessary phase equilibrium and parameter fitting procedures. The FORTRAN program was validated against an existing program, developed independently: the XSEOS thermodynamic computational package for Excel ® [46]. These comparisons were made for systems with a single pore diameter and in which there is no condensation within the pore. In order to compare between the two programs, the objective function in the FORTRAN program was based on the adsorbed amount as given below:

$$f_{obj} = \sum_{k=1}^{n_{\exp}} \left(q_{k,calc} - q_{k,\exp} \right)^2 \qquad (3.1)$$

where $n_{\exp}$ is the number of experimental data points, $q_{k,\exp}$ and $q_{k,calc}$ are the experimental and calculated adsorbed molar amounts (mol/kg) at point k of the experimental data. The objective function represented by equation 3.1 was used previously by Warrag [5].

The objective function f_{obj} in equation 3.1 was minimized under the constraint of equal fugacities of the bulk phase fluid and confined fluid, which is referred to as the isofugacity condition. This constraint is equivalent to imposing that the corresponding chemical potentials are equal. This condition must hold in order to establish adsorption equilibrium. The isofugacity equation is presented as follows:

$$f_{k,calc}\left(T, v_{k,calc}\right) - f_k^{bulk}\left(T, P_k^{bulk}\right) = 0 \qquad (3.2)$$

where $v_{k,calc}$ is the molar volume of fluid confined in the pore, P_k^{bulk} is the specified bulk pressure and, $f_{k,calc}$ and f_k^{bulk} are the fugacities of the confined fluid and bulk phase fluid respectively.

The situation becomes more complex when there is capillary condensation. The typical representation of the adsorption isotherms of pure components is a plot that shows the effect of bulk phase pressure on the adsorbed amounts. When there is capillary condensation in a solid with single pore size, the bulk phase pressure remains constant as long as there are two fluid phases inside the pores. Therefore, for a given P_k^{bulk}, there are multiple possible values for $q_{k,calc}$, which means that the formulation represented by equations (3.1) and (3.2) becomes inapplicable. In order to handle adsorption systems with tendency to capillary condensation, it is convenient to formulate and use a new objective function that takes advantage of the fact that each value of $q_{k,calc}$ corresponds to a single P_k^{bulk} value. It is based minimizing the square of the pressure difference between the experimental data and calculated values while the adsorbed molar amounts are

specified. In this way, the procedure is applicable to systems with a single phase inside the pores and with multiple phases inside the pores. The following equations represent the new objective function and isofugacity equations when a single phase is present inside the pore, respectively:

$$f_{obj} = \sum_{k=1}^{n_{\exp}} \left(P_{k,calc}^{bulk} - P_{k,\exp}^{bulk} \right)^2 \tag{3.3}$$

$$f_{k,calc}\left(T, v_{k,\exp}\right) - f_k^{bulk}\left(T, P_{k,calc}^{bulk}\right) = 0 \tag{3.4}$$

where $P_{k,calc}^{bulk}$ and $P_{k,\exp}^{bulk}$ are the calculated and experimental bulk phase pressures at point k of the experimental data, and $v_{k,\exp}$ represents the experimental molar volume inside the pore, which can be determined from experimental adsorbed amount and the available pore volume. When multiple phases are present inside the pore, equation (3.3) still holds but it is necessary to extend the isofugacity conditions. For example, when there are a vapor-like and a liquid-like phase inside the pore, the isofugacity conditions take the following forms:

$$f_{k,calc}\left(T, v_{k,calc}^{L}\right) - f_k^{bulk}\left(T, P_{k,calc}^{bulk}\right) = 0 \tag{3.5}$$

$$f_{k,calc}\left(T, v_{k,calc}^{V}\right) - f_k^{bulk}\left(T, P_{k,calc}^{bulk}\right) = 0 \tag{3.6}$$

where $v_{k,calc}^{L}$ and $v_{k,calc}^{V}$ represent the calculated liquid-like and vapor-like molar volumes inside the pores at point k of the experimental data, respectively. The values of are such that $v_{k,calc}^{L}$ and $v_{k,calc}^{V}$:

$$\alpha v_{k,calc}^{V} + (1-\alpha) v_{k,calc}^{L} = v_{k,\exp} \tag{3.7}$$

where α denotes the vaporized fraction within the pores.

From the discussion above, it is clear that determining the number of phases inside the pore plays a major role on the calculation path and on the evaluation of the objective function, equation (3.3). The calculation procedure adopted in this work uses a nested-loop approach. The inner loop uses a method of multiphase flash calculation developed by Cabral *et al.* [47] to solve the formulated adsorption equilibrium problem. This is achieved by minimizing the Helmholtz free energy (A) of the system with specified values of T, V, N (i.e. temperature, bulk and pore volumes, and mole numbers of each species). The procedure starts by local minimization of A for a given number of phases as the initial solution. This is followed by a global phase stability analysis, which determines whether the solutions corresponds to a thermodynamically stable state [48]. If the state is found to be stable, it represents the global minimum of the Helmholtz free energy. If the global phase stability test determines that the system is unstable, it also indicates whether to split a bulk phase or a confined phase. After that, the local minimization of A and the global phase stability test are carried out sequentially again, and the procedure is repeated until a stable state is found. This completes the inner loop, whose outcomes include the bulk phase pressure and the amounts in the bulk phase(s) and in the phase(s) inside pore. From the latter, it is possible to compute the value of $q_{k,calc}$, which is the calculated adsorbed molar amount (mol/kg) at point k of the experimental data experimental. If this value is equal to $q_{k,\exp}$, within a pre-defined tolerance, the calculated bulk pressure $P_{k,calc}^{bulk}$ is used in the objective function, equation (3.3). If $q_{k,calc}$ is different from $q_{k,\exp}$, a new value is

specified for N, the number of moles, in the inner loop, and the process is repeated until $q_{k,calc}$ matches $q_{k,\exp}$. Thus, both the parameter fitting and the equilibrium calculation were carried out simultaneously in the FORTRAN program.

This calculation is the core of the parameter fitting procedure; however, other steps are necessary. The following section summarizes them towards the primary goal of modeling fluid behavior in solids with representative bipore size distributions.

3.1 Research procedures

The main tasks to fulfill the goal of the research were:

1. Conduct an extensive literature survey of equations of state models for confined fluids, pore size distribution, and effect of heterogeneous porous structure on Fischer-Tropsch catalytic systems.
2. Identify and study the equation of state for confined fluid that was employed for the research analysis.
3. Collect experimental adsorption data for solid adsorbents from the literature and conduct analysis for pore size distribution using the BJH method.
4. Fit the experimental adsorption data in the selected thermodynamic model to estimate adjustable parameters and carry out multi-phase equilibrium calculations for the bulk and confined fluid in the system at specified conditions**.**
5. Identify the number of fluid phases formed in the bulk and inside the pore at specified conditions to check for pore condensation pore.

6. Compare the results obtained from unipore type with that of multipore type representation.

3.2 Equilibrium calculations and parameter fitting

The PR EOS for confined fluids has two adjustable parameters as mentioned earlier: the characteristic size and energy parameters. They were estimated by fitting to experimental adsorption data. Due to the complexity of the problem, a FORTRAN program written for multiphase equilibrium calculations and parameter fitting were used. The FORTRAN algorithm utilized the simplex method based algorithm, developed by Nelder and Mead [49] to minimize the objective function, while solving the equilibrium equation at each data point using the procedure describer earlier in this chapter. The following are the summary of the steps involved:

1- Collect the experimental adsorption isotherm data for of pure components adsorbed on a solid adsorbents. This is basically the adsorbed amounts corresponding to their pressures as well as the adsorbent characteristic information such as average pore radius and specific pore area and volume.

2- Set the running mode to run over a density range or parameter fitting as required and specify the number of pore type available.

3- Specify the initial estimates of the bulk density assuming the pores are empty, bulk pressure, specific pore volume and molecule-wall interaction parameters.

4- Calculate the adsorbed amount in the confined spaces by fitting the calculated pressures with the experimental data as the bulk density varies.

5- Carryout the optimization of the objective function by changing the characteristic parameters and adsorbed phase pressure, under the constrained of equal fugacities in the bulk and confined phases.

The summary of the multiphase equilibrium calculation using the FORTRAN program is depicted in the algorithm as shown in Figure 5. The program specifications and outcomes are presented in the algorithm chart.

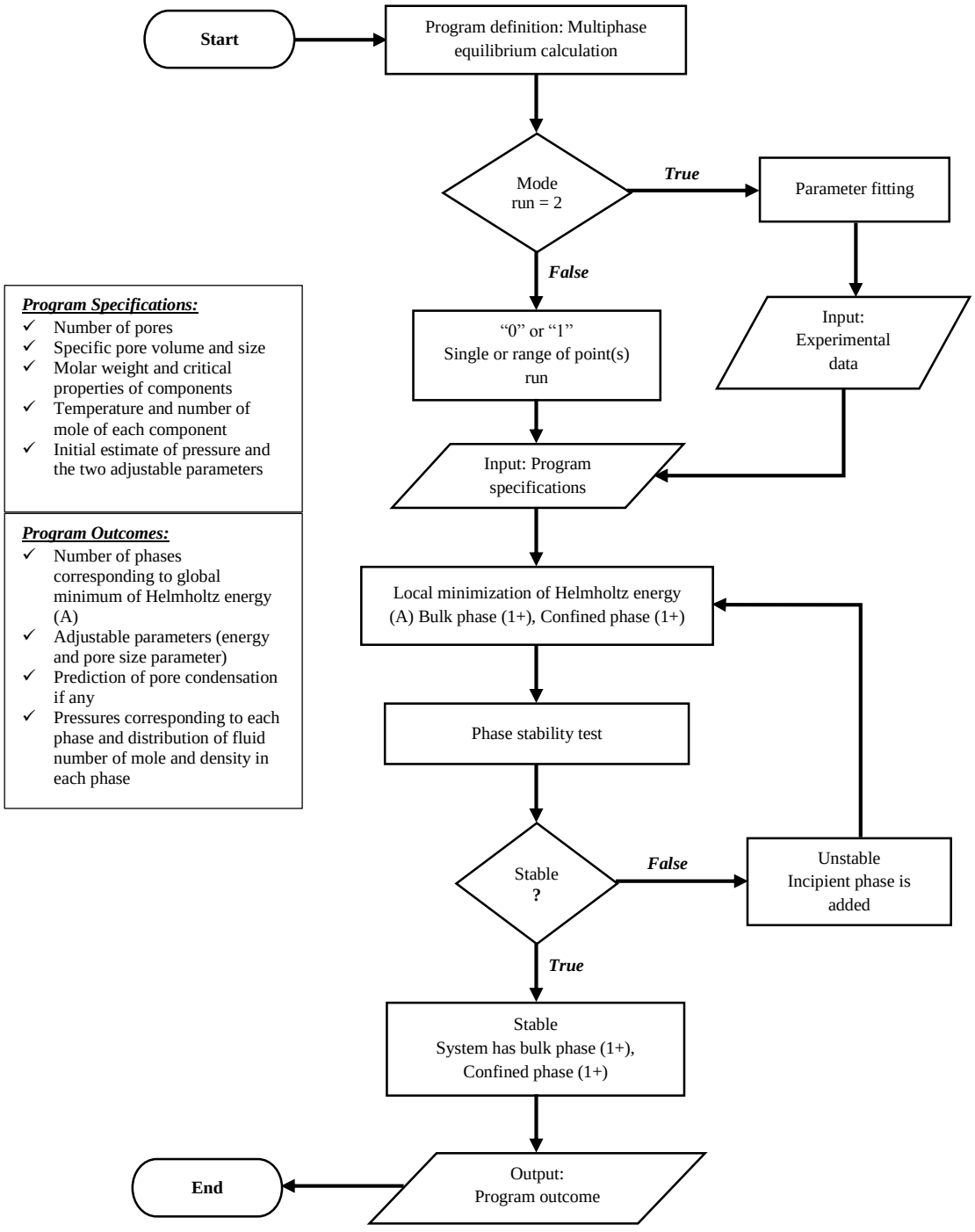

Figure 5: Flow chart of the multiphase equilibrium calculation algorithm

4. RESULTS AND DISCUSSION

This section presents the results of the thesis. The main objective of this work is to investigate the effect of pore size distribution on the phase behavior of fluids in porous structures. This requires a series of rigorous adsorption data fitting and phase equilibrium calculations. A robust FORTRAN program was developed to handle such calculations due to its capacity and speed, and validated with an existing program.

4.1 Program validation

The FORTRAN program was validated by comparing the results with those obtained by Warrag [5] using the Excel XSEOS package [46] for pure components adsorption data fitting on activated alumina and parameter estimation. The results from the FORTRAN program were found to be in excellent agreement with the Excel EOS package. Table 1 shows the summary of the results obtained from the FORTRAN program and Excel EOS Package for methane at 323.15 K, and propane and butane at 313.15 K. Methane was adsorbed on multi-walled carbon nanotube with 0.43 cm^3/g pore volume, 40-60 nm inner pore diameter and 70-100 nm outer pore diameter [50]. Propane and butane were adsorbed on activated alumina with 0.45 cm^3/g pore volume and 4.74 nm pore size [51]. For simplicity of analysis, Warrag [5] used an average pore size of 4.74 nm for the parameter fitting, which was also adopted in this work for the purpose of program validation.

Table 1: FORTRAN program validation with Excel XSEOS package

Components	Objective Function		ε_p/k		δ_P/σ	
	Excel EOS	FORTRAN	Excel XSEOS	FORTRAN	Excel XSEOS	FORTRAN
Methane	7.0741E-03	7.0753E-03	798.0	798.0	0.8804	0.8811
Propane	8.8186E-04	8.8180E-04	1254.2	1254.2	0.7156	0.7162
Butane	1.7556E-04	1.75E-04	1279.7	1279.6	0.3482	0.3488

Figure 6, 7 and 8 show the adsorption data fitting of methane, propane and butane respectively using both Excel XSEOS package and FORTRAN program. It can be seen that the curve generated from the FORTRAN program overlaps on that of the Excel XSEOS package, which implies an accurate match between the two programs.

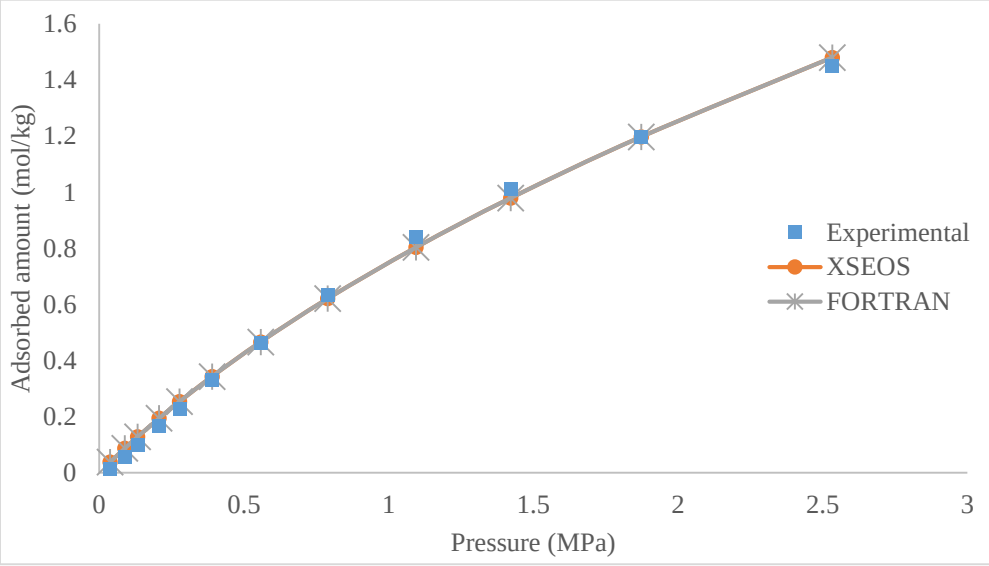

Figure 6: Parameter estimation for methane on activated alumina at 323.15 K using Excel XSEOS package and FORTRAN program [50].

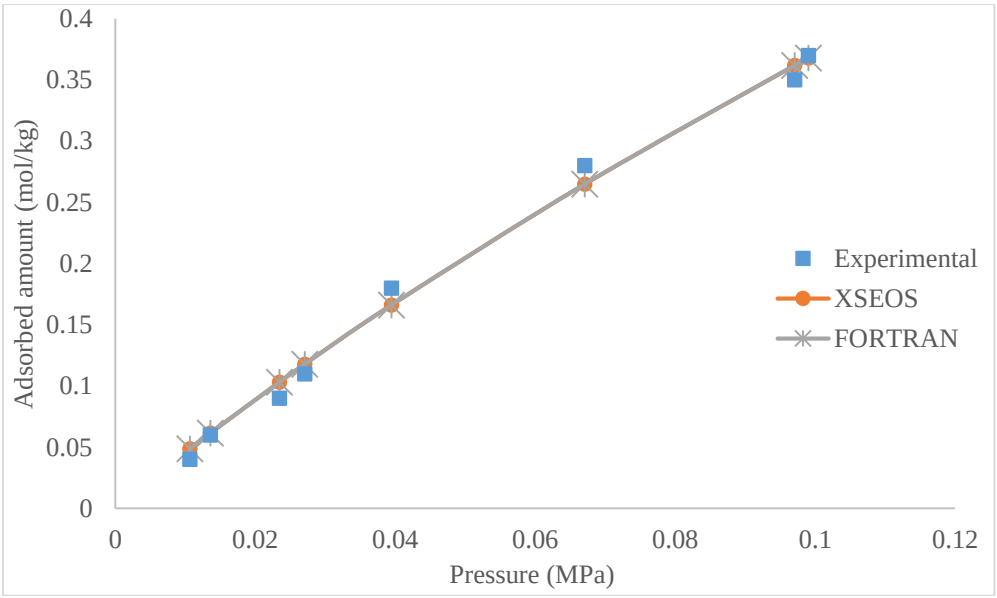

Figure 7: Parameter estimation for propane on activated alumina at 313.15 K using Excel XSEOS package and FORTRAN program [51].

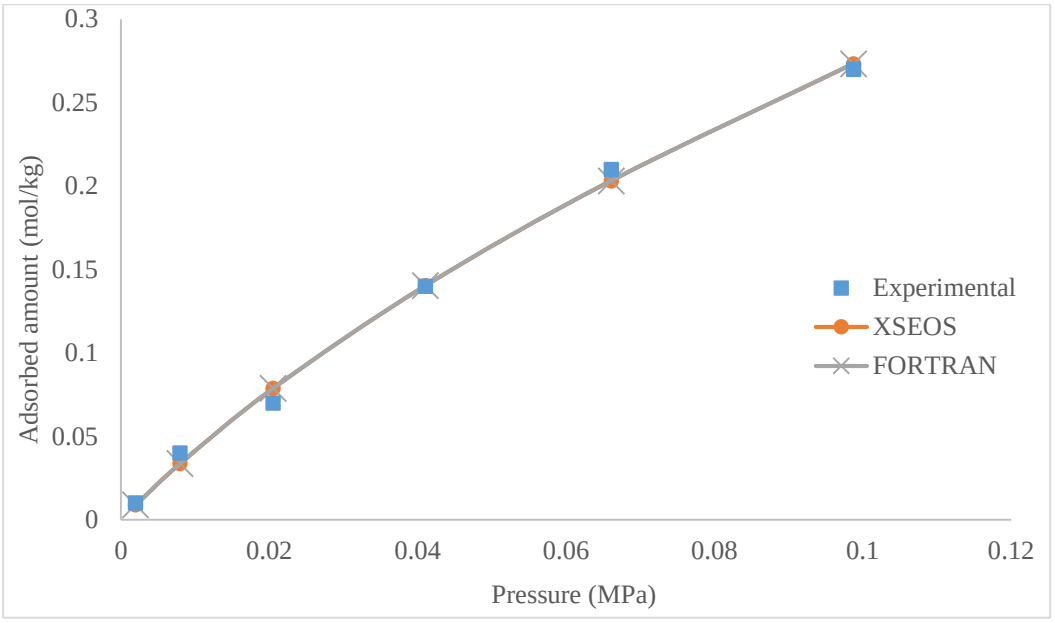

Figure 8: Parameter estimation for butane on activated alumina at 313.15 K using Excel XSEOS package and FORTRAN program [51].

4.2 Illustration of pore size distribution

The experimental adsorption data of pure components were obtained from different sources. Data of pure polar (acetone and methanol) and non-polar (hexane, cyclohexane and benzene) organic components adsorbed on MCM-48 at 303.15, 313.15 and 323.15 K are from Lee *et al.* [52], nitrogen adsorbed on alumina at 77.35 K are from Li *et al.* [44] and methane adsorbed on Zeolite ZSM – 5 at 276.95, 307.95 and 352.75 K are from Sun *et al.* [53]. The analysis of pore size distribution was done using the BJH modified method as presented by Barrett *et al*. and Dollimore & Heal [27, 28]. Figure 9 shows the pore size distribution profile of the conventional unimodal alumina support for FTS.

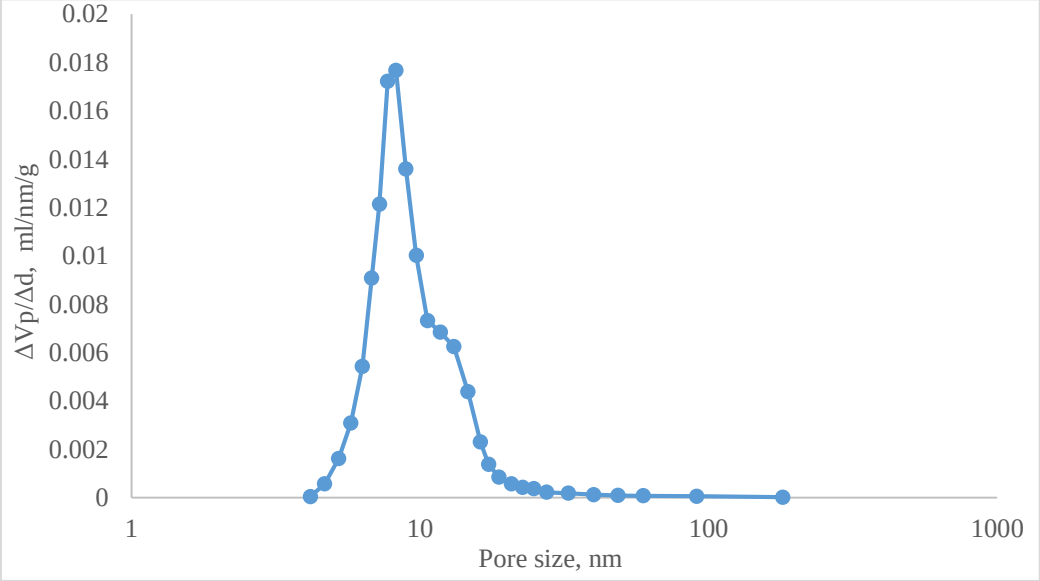

Figure 9: Pore size distribution for unimodal conventional alumina support (Alumina-C) [44].

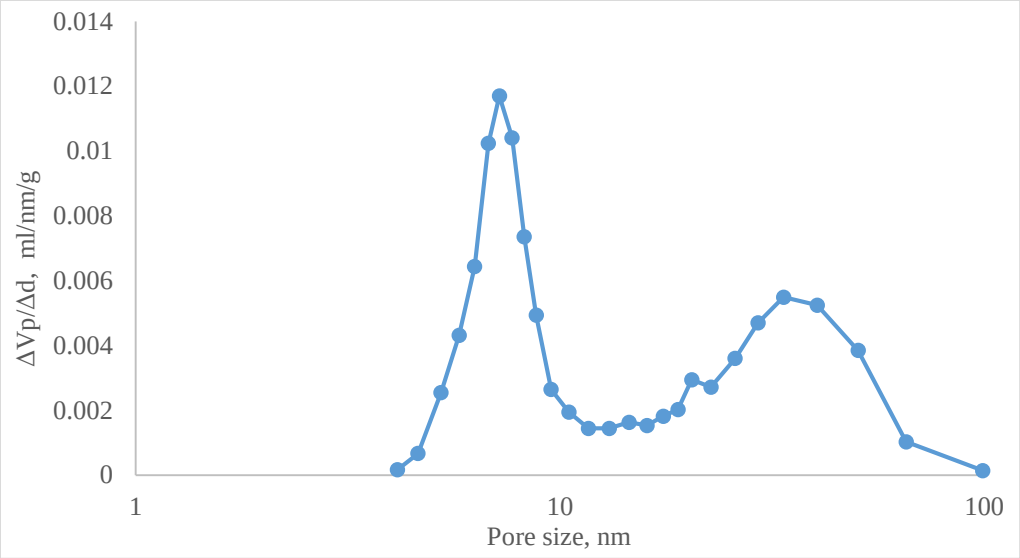

Figure 10: Pore size distribution for bimodal alumina support (Alumina-H) [44].

Figure 10 shows the pore size distribution profile of a typical bimodal alumina support. The parameters such as specific pore volume and average pore size corresponding to each pore type of the unimodal and bimodal alumina support can be calculated from the pore size distribution curves and used as input for the EOS-based modeling of adsorption equilibrium.

4.3 Effect of pore size distribution on adsorption isotherm

The effect of pore size distribution of adsorbents was investigated by using the adsorption isotherm of pure components, i.e. the plot of adsorbed amount (mol/kg) against bulk pressure (MPa). The deviation between the calculated and experimental bulk pressure was set as the objective function. The adsorption data of pure components were fitted through the minimization of the objective function to obtain the two adjustable parameters of the model, i.e. ε_p and δ/σ.

4.3.1 Adsorption of pure components on MCM-48

The adsorption data of some polar and non-polar pure components on MCM-48 were measured experimentally at 323.15 K [52]. The mesoporous MCM-48 adsorbent was characterized with an average pore diameter of 32 Å and pore volume of 1.08 cm^3/g [52]. These data were fitted to obtain the model parameters by considering the cases of unipore and bipore as a representative pore size distribution. The summary of the results is shown in Table 2. It presents the experimental adsorption temperature and pressure range [52], the obtained value of the model adjustable parameters from fitting (δ/σ and ε_p), the average relative deviation (ARD) and the component category.

The MCM-48 adsorbent was assumed to have cylindrical pore geometry in order to fit the adsorption data for single pore and bipore sizes. For bipore fitting, the total pore volume was assumed to be distributed equally (0.54 cm^3/g) into two discrete pore size distributions (20 Å and 44 Å) by offsetting the average pore size. Figure 11 and 12 shows the adsorption data fitting for Acetone on unipore and bipore MCM-48 at 323.15 K using FORTRAN program respectively.

Table 2: Adsorption data fitting for pure polar and non-polar component on MCM-48 results.

Component/Pore size distribution	Experimental		ε_p	δ/σ	ARD (%)	Category
	T (K)	P (MPa) range				
Acetone (Unipore)	323.15	1.22E-04 - 3.14E-02	4702.4	0.3516	22.7	Polar
Acetone (Bipore)	323.15	1.22E-04 - 3.14E-02	4290.7	0.2266	13.1	Polar
			3016.6	0.5269		
Methanol (Unipore)	323.15	3.62E-04 2.05E-02	3416.6	0.4433	23.6	Polar
Methanol (Bipore)	323.15	3.62E-04 - 2.05E-02	3200.2	0.3553	7.7	Polar
			2669.3	0.5707		
Benzene (Unipore)	323.15	1.42E-04 - 1.40E-02	2864.4	0.4952	17.8	Non-polar
Benzene (Bipore)	323.15	1.42E-04 - 1.40E-02	2254.3	0.3784	5.9	Non-polar
			3085.6	0.5512		
Cyclohexane (Unipore)	323.15	6.51E-04 - 1.51E-02	1945.6	0.5985	12.5	Non-polar
Cyclohexane (Bipore)	323.15	6.51E-04 - 1.51E-02	1723.9	0.4324	4.4	Non-polar
			2245.0	0.6773		
Hexane (Unipore)	323.15	6.82E-04 - 2.20E-02	2033.5	0.5634	16.5	Non-polar
Hexane (Bipore)	323.15	6.82E-04 - 2.20E-02	1900.5	0.3728	4.5	Non-polar
			2298.7	0.6724		

It was observed that the largest ARD often occurred at lower bulk pressures. This can be attributed to the effect of squared absolute deviation as tends to distribute the errors evenly for all points, thereby yielding larger percent deviations for small adsorbed values.

For the polar components, it can be observed from Table 2 that the energy parameter (ε_p) of acetone was higher than that of methanol which corresponds to higher molecular interaction energy. However, no clear trend could be established for the size parameter (δ/σ). Generally, the energy parameters obtained from fitting polar components

are higher in comparison with the non-polar components. This can be attributed to their higher values of dipole moment.

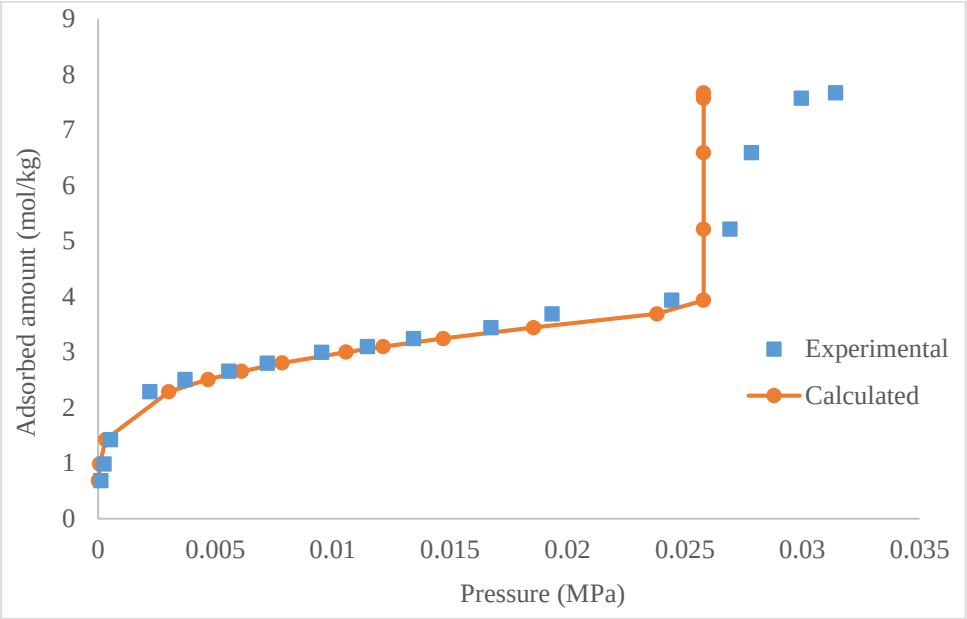

Figure 11: Adsorption data fitting for acetone on unipore MCM-48 at 323.15 K [52].

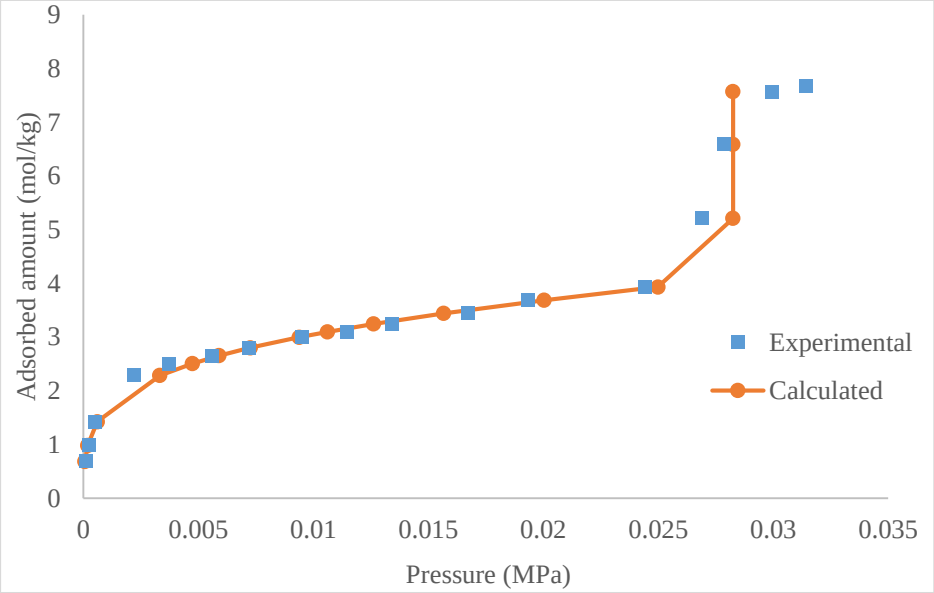

Figure 12: Adsorption data fitting for acetone on bipore MCM-48 at 323.15 K [52].

For the pure acetone fitting on unipore MCM-48 adsorbent, as shown in Figure 11, the model fits the data quite well at lower pressures until about 1.9342E-02 MPa, just before the turning point. The model predicted a drastic equilibrium phase transition at 3.934 mol/kg, which is represented by the vertical line in the calculated curve. This is of no surprise, as such behavior is expected during phase transition when the model is applied to a pure fluid confined within the pores of a solid with single size distribution. The acetone fitting for the bipore pore type in Figure 12 resulted in a better fit between the experimental adsorption data and calculated values with an ARD of 13.1 %. Capillary condensation was indicated by the model at 3.934 mol/kg adsorbed amount following the experimental data, above which there is a slight overestimation and underestimation of bulk pressures.

Figure 13 shows the adsorption data fitting for methanol on unipore MCM-48 adsorbent with 23.6 % ARD. Underestimation of pressures were observed at lower bulk phase pressures until about 3.079 mol/kg adsorbed amount after which pressure were overestimated. The model predicted a phase transition at 4.338 mol/kg which is contrary to the experimental data.

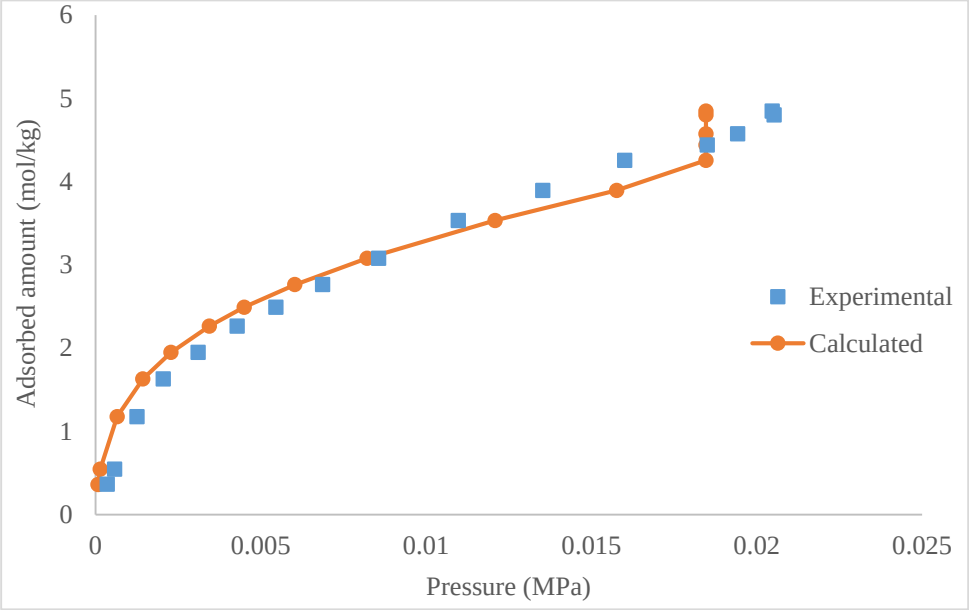

Figure 13: Adsorption data fitting for methanol on unipore MCM-48 at 323.15 K [52].

The model fits excellently well with the methanol experimental adsorption data for bipore MCM-48 solid as depicted in Figure 14, with an ARD of 7.7 %. There is no any indication of capillary condensation in the model prediction, in agreement with the experimental data points.

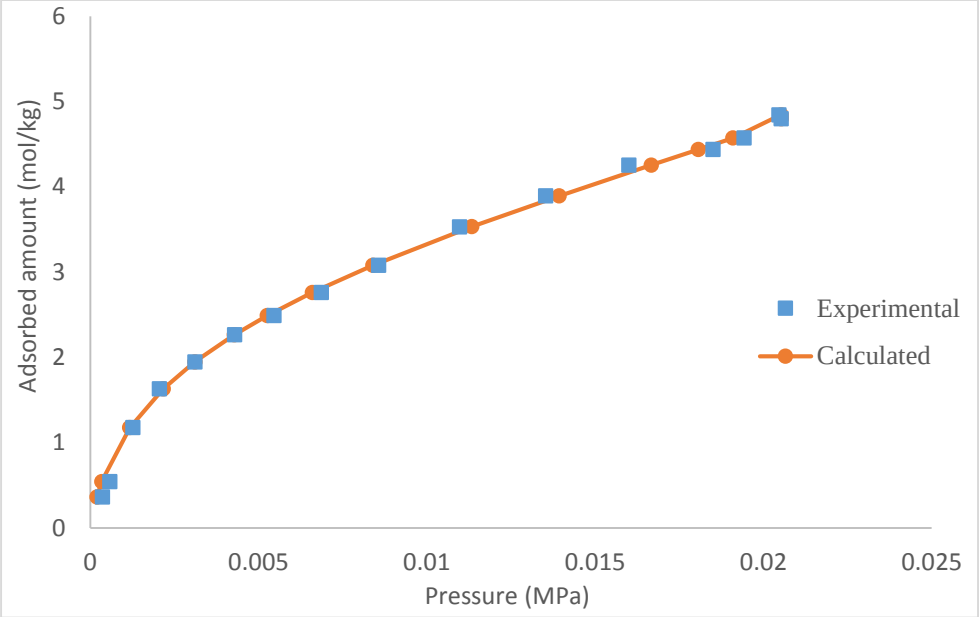

Figure 14: Adsorption data fitting for methanol on bipore MCM-48 at 323.15 K [52].

The fit of benzene on unipore type MCM-48 solid has an ARD of 17.8 %. There is qualitatively poor fit between the experimental and calculated data, as shown in Figure 15, despite the small value of its ARD. There is an equilibrium phase transition starting at 3.26 mol/kg adsorbed amount, indicated by the vertical line of the calculated curve. In contrast, the experimental data shows a gradual change at the point of phase transition with likelihood of metastable equilibrium condition.

Figure 16 represents the benzene fit on bipore MCM-48 solid. The model fits well with the experimental data, with an ARD of 5.9 %, especially at lower pressures before the phase transition and at higher pressures, after the phase transition. At about 3.649 mol/kg, the model followed the gradual transition into liquid-like phase as the experimental data, however with a small deviation.

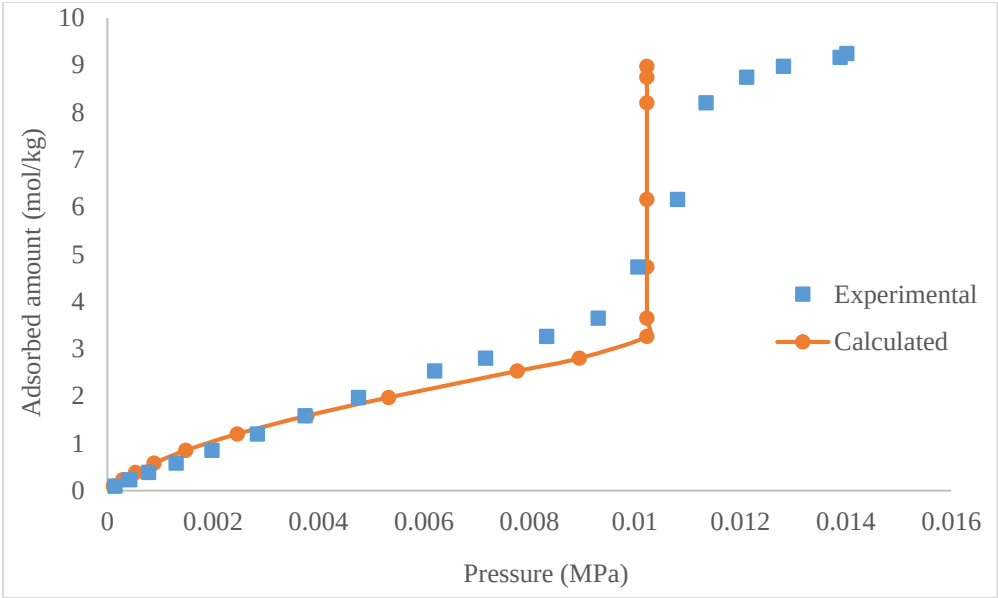

Figure 15: Adsorption data fitting for benzene on unipore MCM-48 at 323.15 K [52].

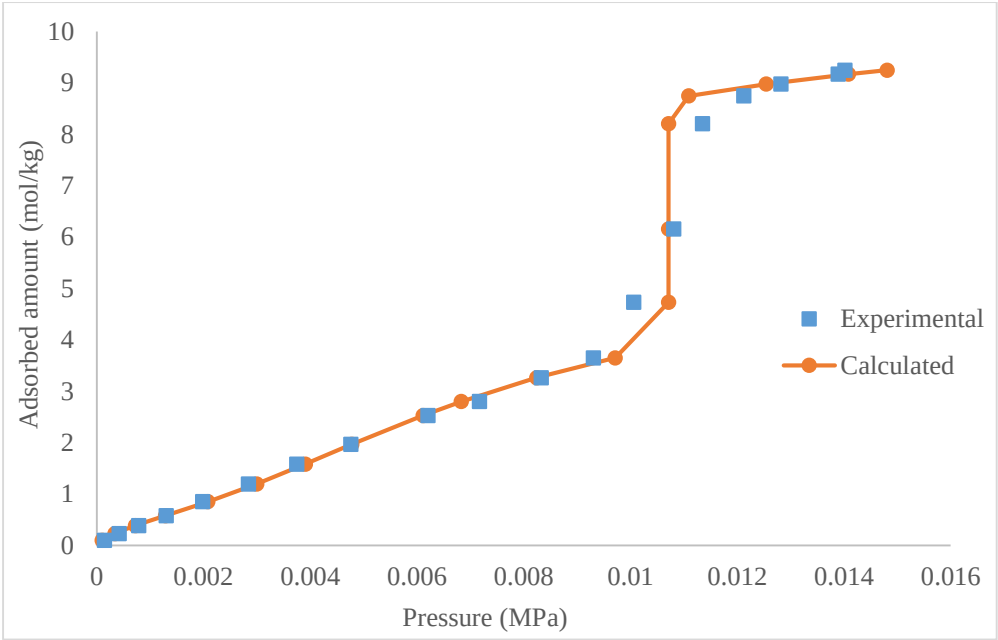

Figure 16: Adsorption data fitting for benzene on bipore MCM-48 at 323.15 K [52].

Figures 17 and 18 show cyclohexane and hexane adsorption data fitting on unipore MCM-48 adsorbent with ARD of 12.5 and 16.5 %, respectively. It can be seen that there is fairly good match at lower pressures until the point of equilibrium phase transition. The model is poorly fitted to the experimental data in both cases at higher pressures.

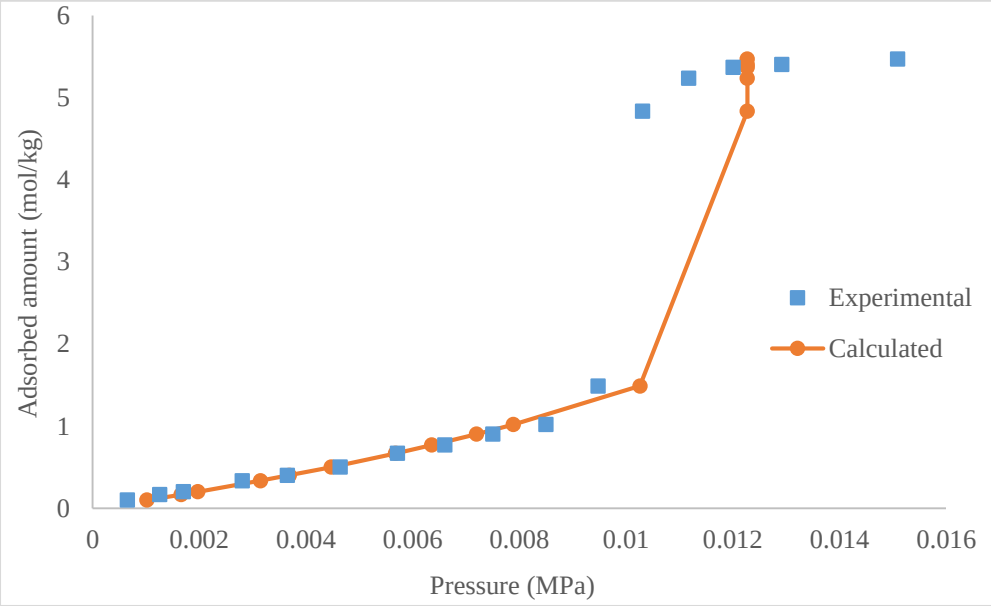

Figure 17: Adsorption data fitting for cyclohexane on unipore MCM-48 at 323.15 K [52].

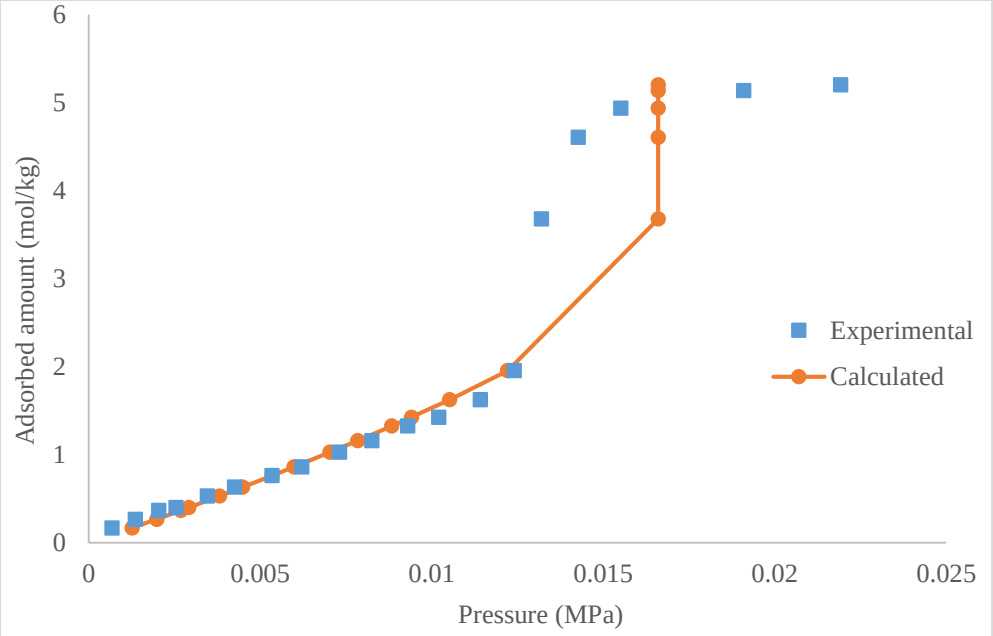

Figure 18: Adsorption data fitting for hexane on unipore MCM-48 at 323.15 K [52].

The fittings for cyclohexane and hexane adsorption data on bipore MCM-48 are respectively depicted in Figures 19 and 20. The ARD of the fittings were estimated to be 4.4 and 4.5 % respectively. The model fits with the experimental data very well, with little deviation of calculated bulk phase pressures at higher adsorption amounts.

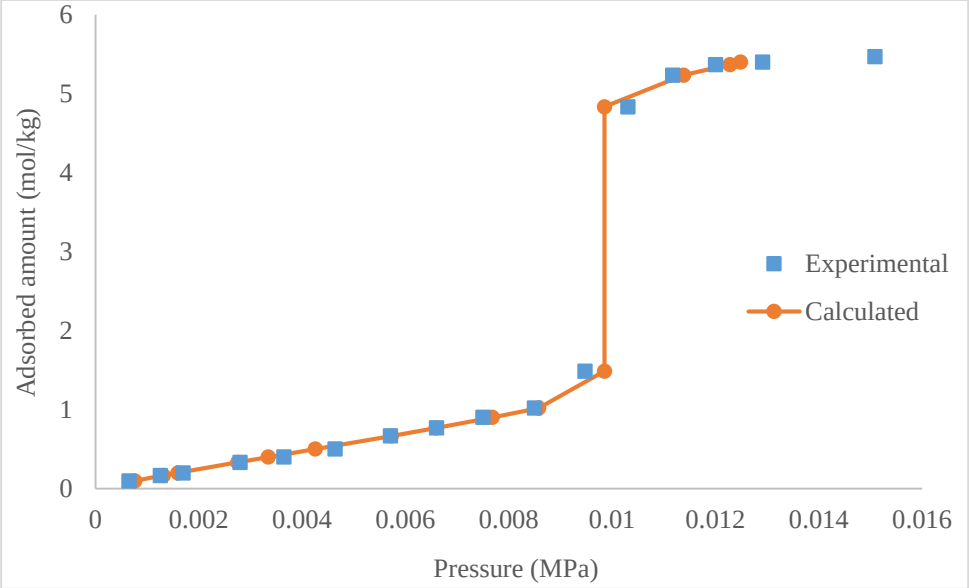

Figure 19: Adsorption data fitting for cyclohexane on bipore MCM-48 at 323.15 K [52].

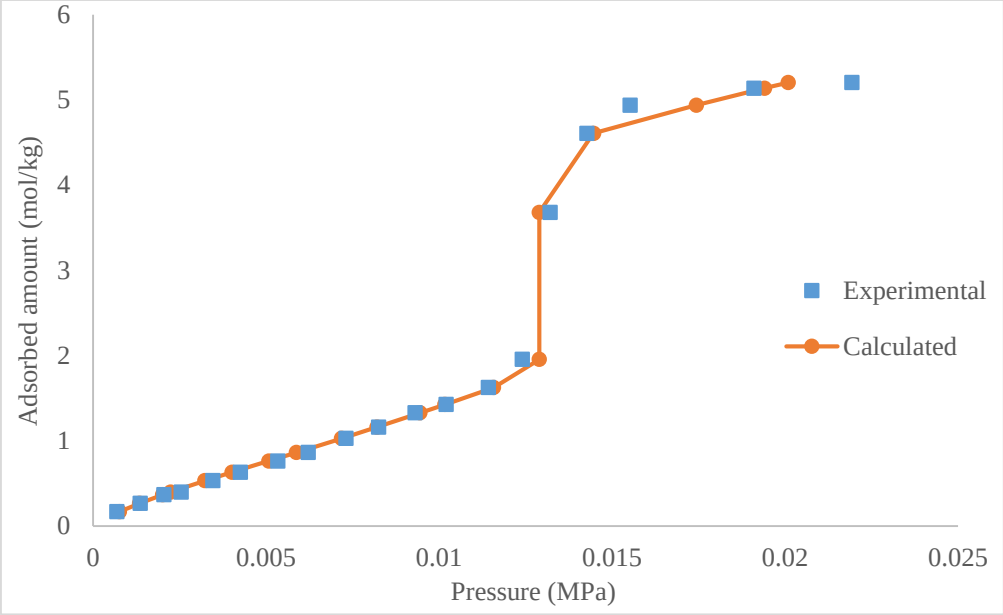

Figure 20: Adsorption data fitting for hexane on bipore MCM-48 at 323.15 K [52].

4.3.2 Adsorption data fitting for multiple pore size distribution

The effect of pore size distribution was further investigated by extending the adsorption parameter fitting and phase equilibrium calculation to higher number of different pore diameters. The adsorption temperature, pressure range and total pore volume were kept the same. For the tripore MCM-48 adsorbent, it was assumed that the total pore volume divided equally (0.36 cm^3/g) into three different pore size distributions (20 Å, 32 Å and 44 Å) around the average pore size. Likewise the multipore MCM-48 adsorbent with four pore sizes, 20 Å, 28 Å, 36 Å and 44 Å pore sizes with 0.27 cm^3/g specific pore volume each were considered.

Table 3: Pure hexane adsorption on multipore MCM-48 results

Component/Pore size distribution	Experimental		ε_p	δ/σ	ARD (%)	Category
	T (K)	P (MPa) range				
Hexane (Unipore)	323.15	6.82E-04 - 2.19E-02	2033.5	0.5634	16.5	Non-polar
Hexane (Bipore)	323.15	6.82E-04 - 2.19E-02	1900.5	0.3728	4.5	Non-polar
			2298.7	0.6724		
Hexane (Tripore)	323.15	6.82E-04 - 2.19E-02	1535.3	0.5825	5.2	Non-polar
			2649.5	0.4417		
			2123.8	0.7128		
Hexane (Quadpore)	323.15	6.82E-04 - 2.19E-02	948.7	0.6580	3.5	Non-polar
			2632.0	0.4813		
			1756.2	0.7371		
			1990.3	0.7651		

Table 3 shows the summary of the adsorption fitting results obtained for hexane on unipore, bipore, tripore and quadpore MCM-48 adsorbent at 323.15 K respectively. Most of the energy parameters obtained from the model have the same order of magnitude

around a value of 2000. A clear trend can be observed in the average relative deviation, ARD column. As the representative number of pore sizes increases, the ARD value reduces which resulted in better fit between the experimental adsorption data and the model at higher number of pores. However, 5.2 % ARD was obtained for the case of tripore which was slightly higher than that of bipore case. This break in the trend can be attributed to the difficulty of getting a suitable initial estimate to fit the parameters.

Figures 21 and 22 show the adsorption isotherm of hexane from experimental data and model prediction considering representative multipore size distributions of three and four number of discrete pores respectively. Following the trend of the adsorption curve fitting in Figures 18, 20, 21 and 22, it was observed that there is tendency of getting more accurate fit as the number of pore sizes increases. This is an indication of the program sensitivity and capability to predict confined fluid behavior in solids with discretized multipore size distribution.

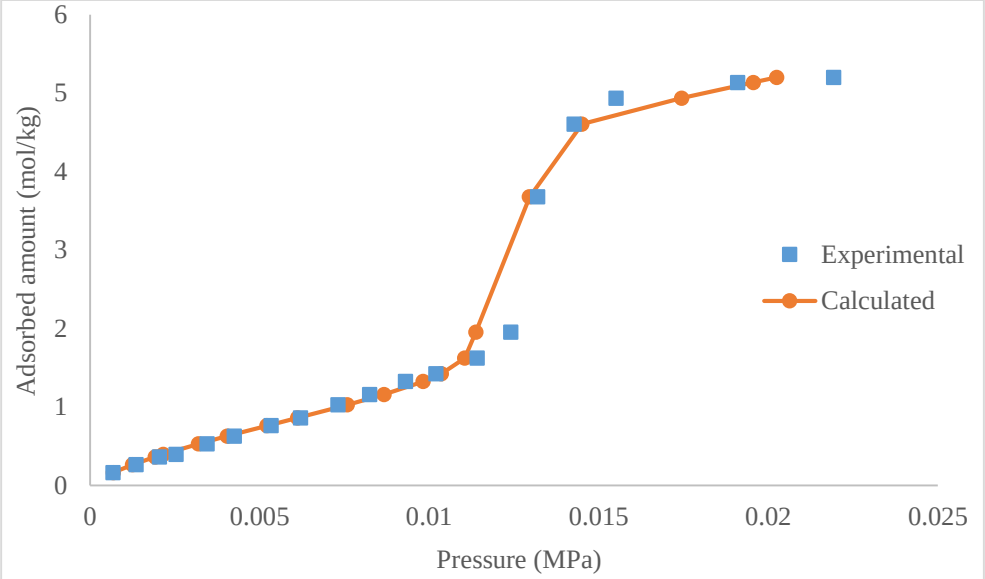

Figure 21: Adsorption data fitting for hexane on tripore MCM-48 at 323.15 K [52].

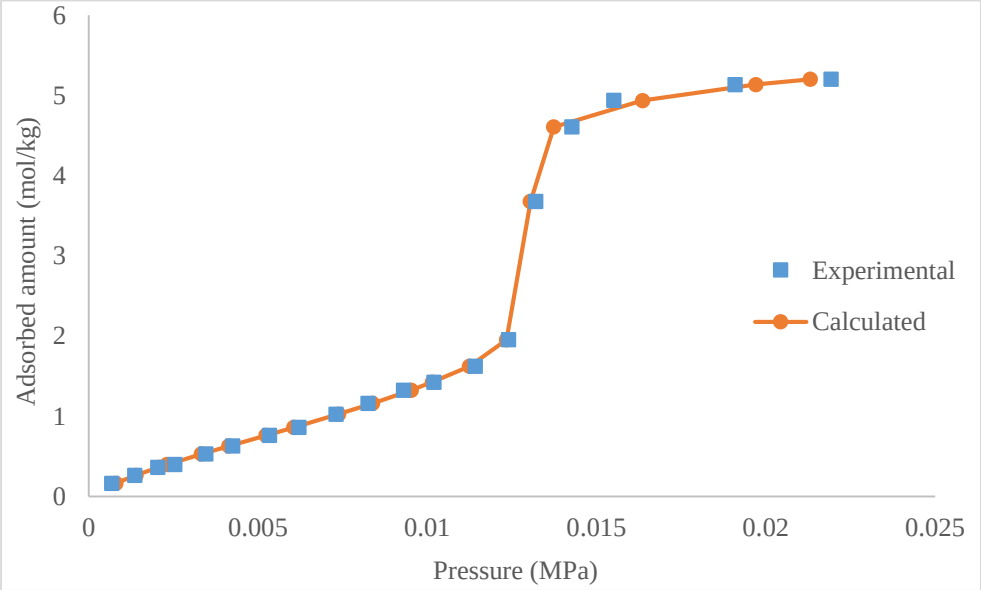

Figure 22: Adsorption data fitting for hexane on quadpore MCM-48 at 323.15 K [52].

Another example is the adsorption data fitting of cyclohexane on MCM-48 silica. Figure 23 shows the NLDFT pore size distribution of MCM-48 silica obtained from argon sorption isotherm at 87 K [54]. The MCM-48 silica was characterized into three discrete pore sizes. The pore sizes are 4.068, 4.540, 5.263 nm corresponding to 0.26, 0.7606 and 0.0436 cm^3/g specific pore volume respectively.

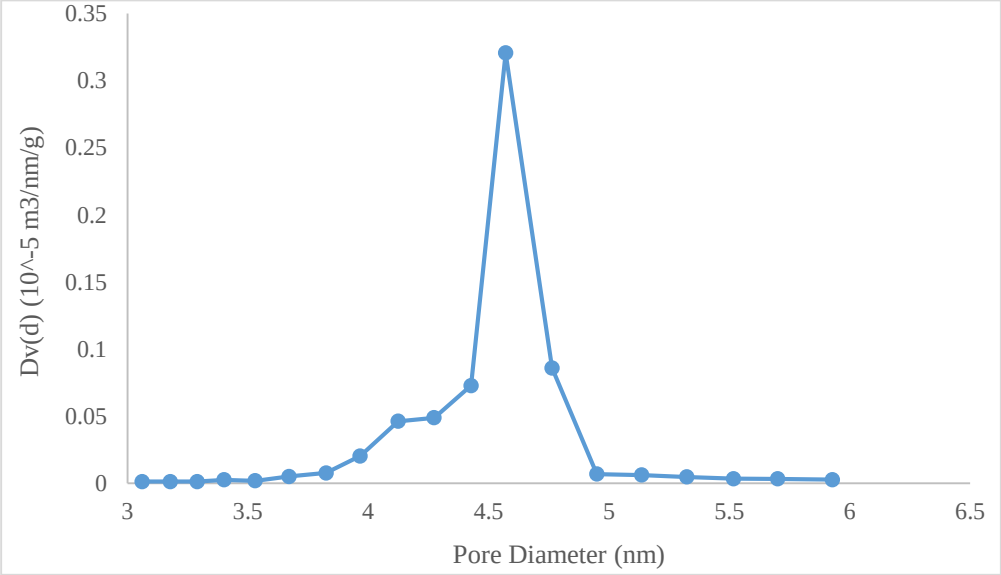

Figure 23: NLDFT pore size distribution curve from argon sorption isotherm on MCM-48 silica at 87 K [54].

Figure 24 illustrate the adsorption data fitting for cyclohexane on tripore MCM-48 silica at 323.15 K. The model fits with the experimental data very well at the beginning of adsorption until approximately 1.5 mol/kg adsorbed amount, where the capillary condensation set in. The model deviate widely at about 5 mol/kg adsorbed amount and could not fall back to the experimental path. There would have been a better set of initial

parameter estimates that will give a better fit. Table 4 presents the set of adjustable model parameters obtained from this fitting. Despite the deviation of the model at the higher adsorbed amount, the 6.1 % ARD value is very small.

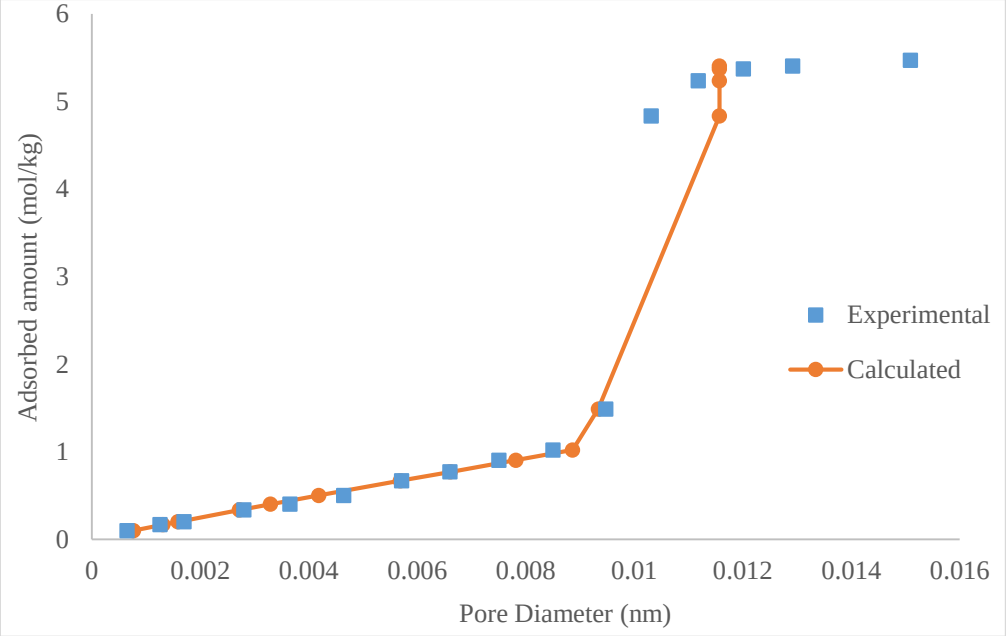

Figure 24: Adsorption data fitting for cyclohexane on tripore MCM-48 silica at 323.15 K [52].

Table 4: Pure cyclohexane adsorption fitting on tripore MCM-48 silica

Component/Pore size distribution	Experimental		ε_p	δ/σ	ARD (%)	Category
	T (K)	P (MPa) range				
Cyclohexane (Tripore)	323.15	6.51E-04 - 1.51E-02	2105.6	0.7023	6.1	Non-polar
			2082.4	0.6813		
			2269.4	0.0399		

4.4 Relationship between bulk phase density and bulk pressure

The pore size distribution has a significant effect on the fluid behavior in a confined space of a porous solid. This phenomenon can be described by showing the relationship between the bulk phase pressure and bulk fluid density. The adsorption of methanol, benzene and hexane on unipore and bipore MCM-48 adsorbent will be used to describe this effect in this section. Figure 25 shows the plots of methanol bulk phase pressure versus density on unipore and bipore MCM-48 solids.

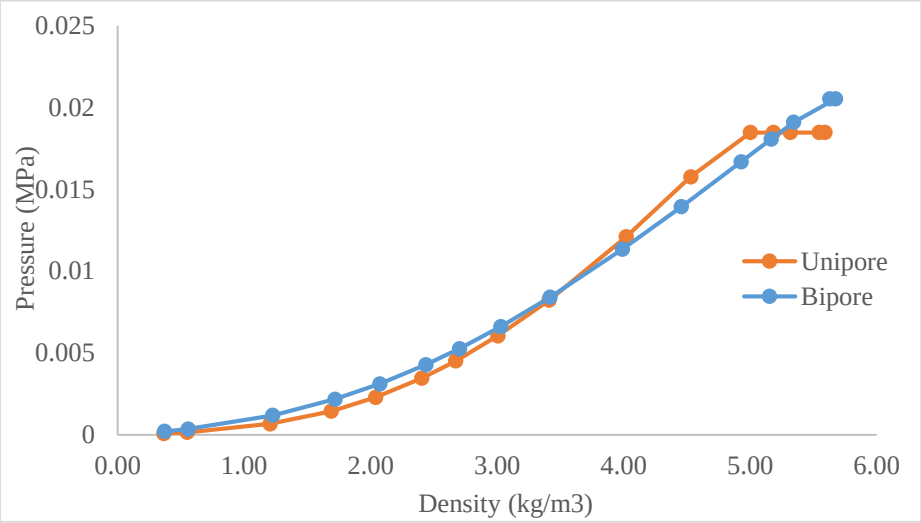

Figure 25: Plot of bulk pressure against density of methanol adsorption on unipore and bipore MCM-48 at 323.15 K.

The model prediction for the methanol adsorption on unipore adsorbent revealed that there exists only one bulk phase and one adsorbed phase as the adsorption proceeds until a bulk pressure of about 1.85E-02 MPa. At this point, the bulk pressure does not increase as the density increases due to the formation of liquid-like dense fluid in the pore.

On the other hand, there is no indication of capillary condensation in the bipore pore type. The bulk pressure increases steadily with density leading to more methanol molecules being adsorbed in the vapor-like phase.

Figure 26 shows the variation between the bulk phase pressure and density for benzene adsorbed on a unipore and bipore MCM-48 adsorbent. There is a smooth trend of increasing gas-like phase adsorption of benzene in both the unipore and bipore solids until the bulk pressures reach approximately 1.02E-02 MPa and remain constant. It can be seen that the bulk phase pressure in the bipore system at the equilibrium phase transition region is slightly higher than in the unipore adsorbent, thereby delaying the formation of two phases in the pores. At about 9.192 kg/m^3 bulk density in the bipore system, a sudden transition is observed, which indicates that there is a single phase in each pore.

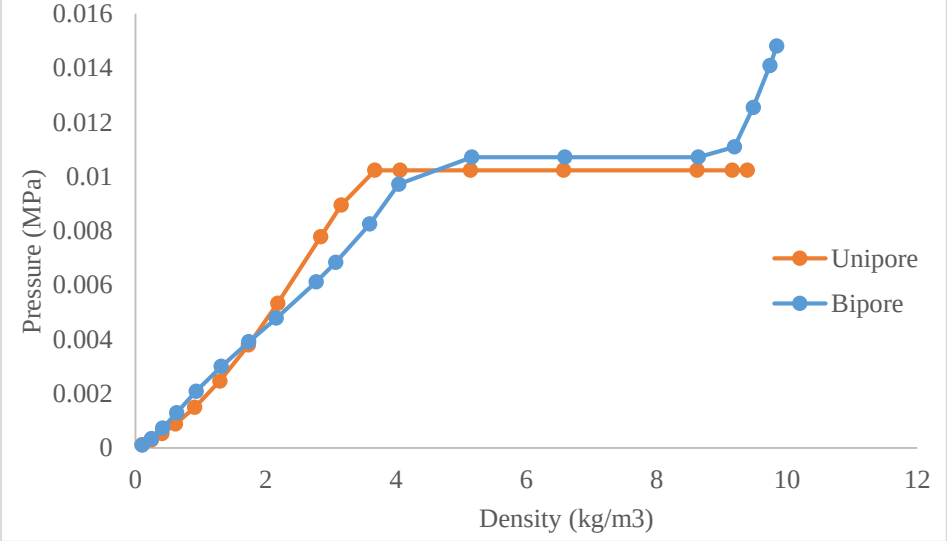

Figure 26: Plot of bulk pressure against density of benzene adsorption on unipore and bipore MCM-48 at 323.15 K.

The phase behavior of hexane in unipore and bipore MCM-48 solid is demonstrated in Figure 27. It follows a similar trend to benzene as described above. However, the capillary pressure in the unipore solid at pore condensation region is slightly higher than that of bipore system. This can be attributed to the different fittings for the unipore and bipore systems.

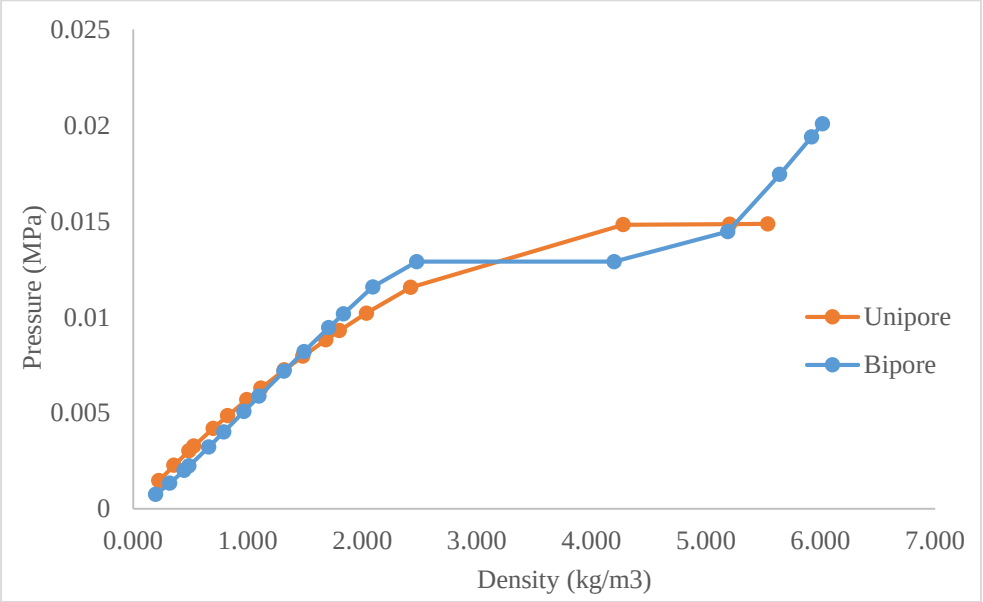

Figure 27: Plot of bulk pressure against density of hexane adsorption on unipore and bipore MCM-48 at 323.15 K.

4.5 Temperature dependence of the model

The effect of temperature on the model relative to pore size distribution was analyzed using the adsorption isotherm of methane on Zeolite ZSM–5. The ZSM–5 has

pore size distribution ranging between 4 – 8 Å with 0.242 cm^3/g specific pore volume as obtained from ZEOMICS [55]. The experimental adsorption data of methane on ZSM–5 at three different temperatures, 276.95 K, 307.95 K and 352.75 K were fitted respectively [53], A representative bipore size distributions with 5.5 Å and 7 Å pore sizes was considered. Table 5 shows the summary of the results obtained from the fitting of methane experimental adsorption data on ZSM–5 at three different temperatures.

Table 5: Pure methane adsorption on ZSM–5 results

Component/Pore size distribution	Experimental		ε_p	δ/σ	ARD (%)
	T (K)	P (MPa) range			
Methane (Bipore)	276.95	4.14E-02 - 2.05E+00	582.8	0.4653	26.4
			2222.8	0.7260	
Methane (Bipore)	307.95	8.55E-02 - 2.06E+00	1625.0	0.2986	19.4
			3734.1	0.1351	
Methane (Bipore)	352.75	8.2E-02 - 2.07E+00	907.8	0.2918	12.1
			1877.0	0.5864	

Figures 28, 29 and 30 show the adsorption data fitting for methane on bipore ZSM-5 at 276.95 K, 307.95 K and 352.75 K respectively. It can be observed that the amount of methane molecules adsorbed corresponding to the bulk pressures decline as the temperature increases as expected. Both the experimental data and the model clearly show the effect of temperature on adsorbed amount.

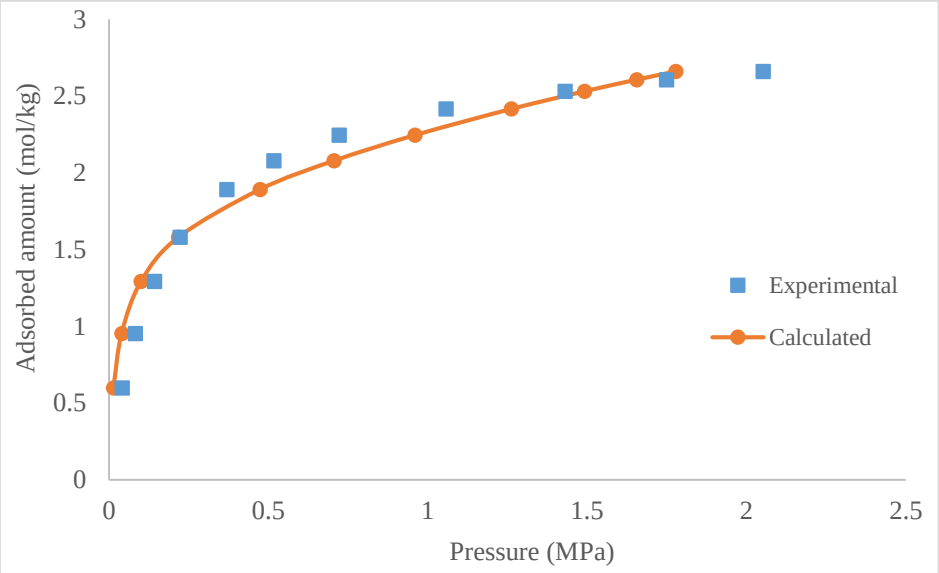

Figure 28: Adsorption data fitting for methane on bipore ZSM-5 at 276.95 K [53].

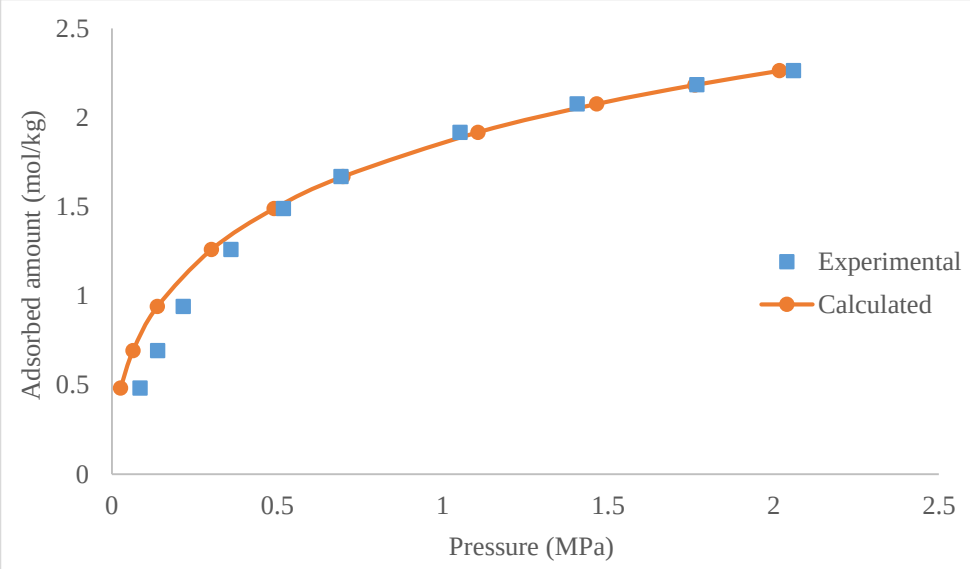

Figure 29: Adsorption data fitting for methane on bipore ZSM-5 at 307.95 K [53].

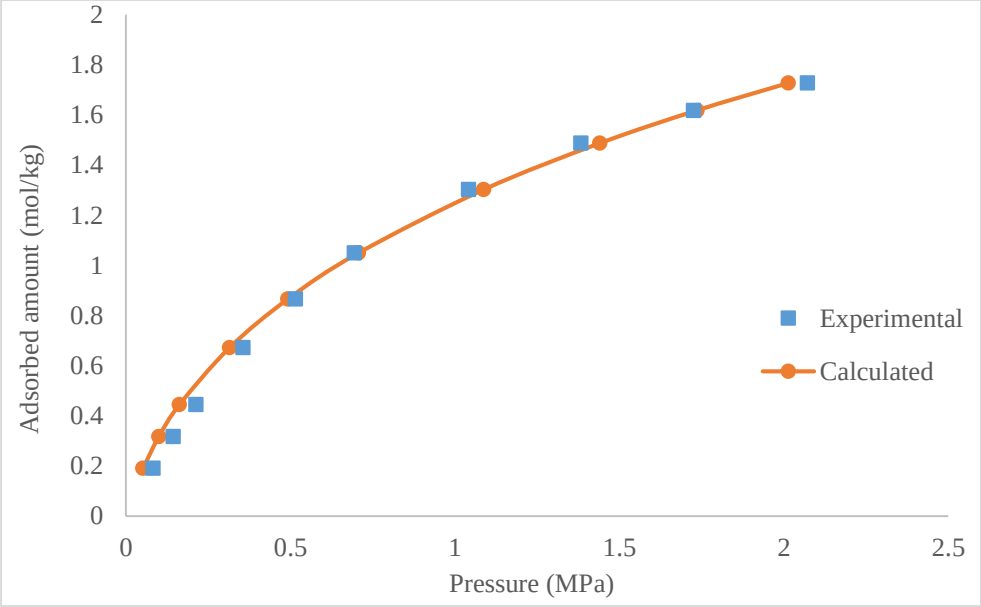

Figure 30: Adsorption data fitting for methane on bipore ZSM-5 at 352.75 K [53].

The above example illustrates the importance of consistent experimental data points from the same source. The sensitivity of the model to adsorption temperature can be established from this example. As the adsorption temperature increases, the accuracy of the fitting increases. The best fitting was obtained from the adsorption data fitting for methane at 352.75 K.

5. CONCLUSION AND FUTURE WORK

5.1 Conclusions

The outcome of this research provided a better understanding of the capabilities of Peng-Robinson equation of state extended to confined fluids when applied to predicting the phase behavior of fluids within materials with different pore size distributions. The multiphase equilibrium calculations were conducted for fluids confined in unipore and bipore solid adsorbent. This led to an interesting set of results about pore condensation vis-à-vis the metastability condition for adsorbed fluids in confinement.

The results obtained from adsorption data fitting revealed that the model correlation for fluids adsorbed in bipore solids was far better than that of the unipore systems at the same temperature and total specific pore volume. There were comparatively excellent matches between the experimental and calculated adsorption data for bipore MCM-48 as indicated by their relatively smaller ARD values. Furthermore, the model predicted equilibrium phase transition leading to capillary condensation in both cases. This is represented by the straight vertical line in the calculated adsorption isotherms, which corresponds to the turning points of the experimental isotherm. This prediction was in good agreement with the result obtained from NLDFT simulations [9].

At the equilibrium phase transition region, the modeling approach used in this work forces the system to the true equilibrium stability state. This effect is more obvious in the unipore systems and may even be predicted earlier than observed in the experimental adsorption isotherm. On the other hand, the experimental adsorption isotherm often

showed delayed vapor-liquid transition as a result of metastability of the confined fluids, which can be attributed to the heterogeneity of the pore size and the non-uniformity degree of the pore channels, according to Neimark and Ravikovitch [9]. This is not captured by the model used here, which is designed to determine the condition of stable thermodynamics equilibrium.

At the end of capillary condensation region, the experimental adsorption isotherm shows further adsorption of fluid molecules in the liquid-like phase. The model also predicts similar trend for bipore porous adsorbent, which can be of high importance in heterogeneous catalysis.

The trend of the temperature dependency of the model was considered. Adsorption data fittings tend to be more accurate as the temperature increases. It is important to note the sensitivity of the fitting procedure to the initial parameter estimates, as this can affect the ability to fit. The recommendation is to try different initial estimates.

Variety of experimental adsorption data from reliable sources may be quite difficult to get. There are also uncertainties associated to the generation of these data due to the complex nature of adsorption experiments. This is one of the major challenges to adsorption modeling, especially for adsorbents with more than one pore size distribution. In other to achieve high level of accuracy and good prediction, reliable sets of data from the same source should be used for model fitting and comparison. The calculation should be repeated for different data sets from different sources to validate the efficiency of the model. In the recent years, attention has been paid to the development and characterization

of bipore solid adsorbent due to its importance and potential applications and modeling their performance will be a topic of increasing relevance.

5.2 Future work

While this work has conceptually shown how the modeling of confined fluids can be improved by accounting for multiple pore sizes, several refinements are possible.

The model can be improved to incorporate the effect of non-homogeneity of adsorbent pores and the degree of its non-uniformity such as interconnected nest-like pores or combination of cylindrical and spherical pores as in zeolite channels and cavities. This will possibly lead to a better prediction of adsorption behaviour, as well as of capillary condensation.

Another area of future work is the application of the model to a specific scenario such as the work of Warrag [5] on "Predictions of Multiphase Equilibrium of Fluids Confined in Fischer-Tropsch Catalyst Porous Structure", however, with higher complexity. Consideration of adsorption of complex mixtures on multimodal porous solids will be an interesting research. The scarcity of experimental data on the thermodynamic behavior of confined FTS fluids is a limiting factor for studies of this type. However, the use of molecular simulation, either Monte Carlo or molecular dynamics, may provide insight into the phenomena that happen in such systems at molecular level. The pseudo-experimental data these methods generate would be used to test the ability of the approach developed in this thesis.

The issue of metastability merits additional investigation. The calculations of this work report results of thermodynamically stable states. A systematic investigation of the

model predictions along a metastable equilibrium path, as experienced when measuring experimental adsorption isotherms, will expand the knowledge about how to apply the model to heterogeneous adsorbents.

Finally, it will be interesting to use the framework to solve the problem of finding the pore size distribution that gives the best possible representation of the confined fluid behavior with the extended Peng-Robinson equation of state.

5.3 Program availability

The computer program used for this work is available upon request.

REFERENCES

[1] S. P. Tan and M. Piri, "Equation-of-state modeling of confined-fluid phase equilibria in nanopores," *Fluid Phase Equilib.*, vol. 393, pp. 48–63, 2015.

[2] L. Travalloni, M. Castier, and F. W. Tavares, "Phase equilibrium of fluids confined in porous media from an extended Peng-Robinson equation of state," *Fluid Phase Equilib.*, vol. 362, pp. 335–341, 2014.

[3] N. Elbashir, D. Bukur, E. Durham, and C. Roberts, "Advancement of Fischer-Tropsch synthesis via utilization of supercritical fluid reaction media," *AIChE J.*, vol. 56, no. 4, pp. 997–1015, 2010.

[4] Yokota and Fujimoto, "Supercritical-phase Fischer-Tropsch synthesis reaction. 2. The effective diffusion of reactant and products in the supercritical-phase reaction," *Ind. Eng. Chem. Res.*, vol. 30, no. 1, pp. 95–100, 1991.

[5] S. E. Warrag, "Multiphase equilibrium of fluids confined in Fisher-Tropsch catalytic systems," *Msc thesis (Unpublished), Texas A&M Univ. Qatar*, 2014.

[6] L. Travalloni, M. Castier, F. W. Tavares, and S. I. Sandler, "Thermodynamic modeling of confined fluids using an extension of the generalized van der Waals theory," *Chem. Eng. Sci.*, vol. 65, no. 10, pp. 3088–3099, 2010.

[7] B. Coasne, C. Alba-Simionesco, F. Audonnet, G. Dosseh, and K. E. Gubbins, "Adsorption and structure of benzene on silica surfaces and in nanopores,"

Langmuir, vol. 25, no. 7, pp. 10648–10659, 2009.

[8] R. R. Kotdawala, N. Kazantzis, and R. W. Thompson, "Analysis of binary adsorption of polar and nonpolar molecules in narrow slit-pores by mean-field perturbation theory," *J. Chem. Phys.*, vol. 123, no. 244709, pp. 1–11, 2005.

[9] A. V. Neimark and P. I. Ravikovitch, "Capillary condensation in MMS and pore structure characterization," *Microporous Mesoporous Mater.*, vol. 44–45, pp. 697–707, 2001.

[10] M. Schoen and D. J. Diestler, "Analytical treatment of a simple fluid adsorbed in a slit-pore," *J. Chem. Phys.*, vol. 109, no. 13, p. 5596, 1998.

[11] A. Giaya and R. W. Thompson, "Water confined in cylindrical micropores," *J. Chem. Phys.*, vol. 117, no. 7, pp. 3464–3475, 2002.

[12] H. Y. Zhu, L. a. Ni, and G. Q. Lu, "Pore-size-dependent equation of state for multilayer adsorption in cylindrical mesopores," *Langmuir*, vol. 15, no. 10, pp. 3632–3641, 1999.

[13] E. G. Derouane, "On the physical state of molecules in microporous solids," *Microporous Mesoporous Mater.*, vol. 104, no. 1–3, pp. 46–51, 2007.

[14] G. J. Zarragoicoechea and V. a. Kuz, "Van der Waals equation of state for a fluid in a nanopore," *Phys. Rev. E - Stat. Nonlinear, Soft Matter Phys.*, vol. 65, pp. 1–4, 2002.

[15] A. W. Islam, T. W. Patzek, and A. Y. Sun, “Thermodynamics phase changes of nanopore fluids,” *J. Nat. Gas Sci. Eng.*, vol. 25, pp. 134–139, 2015.

[16] Y. Ma and A. Jamili, “Modeling the density profiles and adsorption of pure and mixture hydrocarbons in shales,” *J. Unconv. Oil Gas Resour.*, vol. 14, pp. 128–138, 2016.

[17] X. Dong, H. Liu, J. Hou, K. Wu, and Z. Chen, “Phase equilibria of confined fluids in nanopores of tight and shale rocks considering the effect of capillary pressure and adsorption film,” *Ind. Eng. Chem. Res.*, 2016.

[18] Y. Li and H. Pu, “Modeling study on CO2 capture and storage in organic-rich shale,” no. November, pp. 17–19, 2015.

[19] K. Dhanapal, D. Devegowda, Y. Zhang, A. C. Contreras-Nino, F. Civan, and R. Sigal, “Phase behavior and storage in organic shale nanopores: Modeling of multicomponent hydrocarbons in connected pore systems and implications for fluids-in-place estimates in shale oil and gas reservoirs,” in *SPE Unconventional Resources Conference*, 2014.

[20] Y. Ma, L. Jin, and A. Jamili, “Modifying van der Waals equation of state to consider influence of confinement on phase behavior,” *SPE 166476*, no. 1966, 2013.

[21] T. L. Hill, *Introduction to statistical thermodynamics*. Dover Publications, 1986.

[22] V. Bolis, *Fundamentals in adsorption at the solid-gas interface. Concepts and*

thermodynamics, A. Auroux., vol. 154. Berlin Heidelberg: Springer Series in Materials Science, 2013.

[23] S. Mao, "NMR studies of gas and water adsorption in carbon based materials," *PhD Diss. Univ. North Carolina Chapel Hill*, 2007.

[24] R. N. Horne, H. J. Ramey, S. Shang, A. Correa, and J. Hornbrook, "The effects of adsorption and desorption on production and reinjection in vapor- dominated geothermal fields," *Proc. World Geotherm. Congr. Florence, Italy, May 1995*, pp. 1973–1977, 1995.

[25] D. H. Everett, "International union of pure and applied chemistry division of physical chemistry manual of symbols and terminology for physicochemical quantities and units appendix II," *Pure Appl. Chem.*, vol. 51, no. 5, pp. 1213–1218, 2001.

[26] S. Lowell, J. E. Shields, M. a. Thomas, and M. Thommes, *Characterisation of porous solids and powders*. New York: Kluwer Academic, 2004.

[27] J. J. Carberry, *Chemical and catalytic reaction engineering*. Dover Publications, 2001.

[28] A. Grosman and C. Ortega, "Nature of capillary condensation and evaporation processes in ordered porous materials," *Langmuir, Am. Chem. Soc.*, vol. 21, no. 2, p. 10515, 2005.

[29] K. Morishige and N. Tarui, “Capillary condensation of nitrogen in ordered mesoporous silica with bicontinuous gyroid structure,” *J. Phys. Chem. C*, vol. 111, no. 1, pp. 280–285, 2007.

[30] M. Thommes, B. Smarsly, M. Groenewolt, P. I. Ravikovitch, and A. V. Neimark, “Adsorption hysteresis of nitrogen and argon in pore networks and characterization of novel micro- and mesoporous silicas,” *Langmuir*, vol. 22, no. 2, pp. 756–764, 2006.

[31] Y. Kim, C. Kim, and J. Yi, “Synthesis of tailored porous alumina with a bimodal pore size distribution,” *Mater. Res. Bull.*, vol. 39, no. 13, pp. 2103–2112, 2004.

[32] J. Y. Ying, C. P. Mehnert, and M. S. Wong, “Synthesis and applications of supramolecular-templated mesoporous materials,” *Angew. Chemie Int. Ed.*, vol. 38, no. 1–2, pp. 56–77, 1999.

[33] J. Rouquerol, D. Avnir, C. W. Fairbridge, D. H. Everett, J. M. Haynes, N. Pernicone, J. D. F. Ramsay, K. S. W. Sing, and K. K. Unger, “Recommendations for the characterization of porous solids (Technical Report),” *Pure Appl. Chem.*, vol. 66, no. 8, pp. 1739–1758, Jan. 1994.

[34] H. Yan, C. F. Blanford, J. C. Lytle, C. Barry Carter, W. H. Smyrl, and a. Stein, “Influence of processing conditions on structures of 3D ordered macroporous metals prepared by colloidal crystal templating,” *Chem. Mater.*, vol. 13, no. 11, pp. 4314–4321, 2001.

[35] J. Sun, Z. Shan, T. Maschmeyer, J. a. Moulijn, and M.-O. Coppens, “Synthesis of tailored bimodal mesoporous materials with independent control of the dual pore size distribution,” *Chem. Commun.*, no. 24, pp. 2670–2671, 2001.

[36] T. R. Pauly, Y. Liu, T. J. Pinnavaia, S. J. L. Billinge, and T. P. Rieker, “Textural mesoporosity and the catalytic activity of mesoporous molecular sieves with wormhole framework structures,” *J. Am. Chem. Soc.*, vol. 121, no. 38, pp. 8835–8842, 1999.

[37] O. Levenspiel, *Chemical reaction engineering*, 3rd ed. New York: Wiley, 1999.

[38] E. P. Barrett, L. G. Joyner, and P. P. Halenda, “The determination of pore volume and area distributions in porous substances. I. Computations from nitrogen isotherms,” *J. Am. Chem. Soc.*, vol. 73, no. 1, pp. 373–380, 1951.

[39] D. Dollimore and G. R. Heal, “An improved method for the calculation of pore size distribution from adsorption data,” *J. Appl. Chem.*, vol. 14, no. 3, pp. 109–114, 1964.

[40] H. Xiong, Y. Zhang, S. Wang, and J. Li, “Fischer-Tropsch synthesis: The effect of Al2O3 porosity on the performance of Co/Al2O3 catalyst,” *Catal. Commun.*, vol. 6, no. 8, pp. 512–516, 2005.

[41] F. Fischer and H. Tropsch, “The preparation of synthetic oil mixtures (synthol) from carbon monoxide and hydrogen,” *Fuel Chem*, vol. 4, pp. 276–285.

[42] J. R. Nimmo, "Porosity and pore size distribution," *Encycl. Soils Environ.*, pp. 295–303, 2004.

[43] Tsubaki, Zhang, S. Sun, Mori, Y. Yoneyama, Li, Fujimoto, N. Tsubaki, Y. Zhang, S. Sun, H. Mori, Y. Yoneyama, X. Li, and K. Fujimoto, "A new method of bimodal support preparation and its application in Fischer-Tropsch synthesis," *Catal. Commun.*, vol. 2, no. 10, pp. 311–315, 2001.

[44] C. Liu, J. Li, Y. Zhang, S. Chen, J. Zhu, and K. Liew, "Fischer-Tropsch synthesis over cobalt catalysts supported on nanostructured alumina with various morphologies," *J. Mol. Catal. A Chem.*, vol. 363–364, pp. 335–342, 2012.

[45] Y. Liu, H. Guo, L. Jia, Z. Ma, Y. Xiao, C. Chen, and M. Xia, "Fischer-Tropsch synthesis over alumina- supported cobalt-based catalysts : Effect of support variables," *J. Mater. Sci. Chem. Eng.*, vol. 2, pp. 19–27, 2014.

[46] M. Castier and M. M. Amer, "XSEOS: An evolving tool for teaching chemical engineering thermodynamics," *Educ. Chem. Eng.*, vol. 6, no. 2, pp. e62–e70, 2011.

[47] V. F. Cabral, M. Castier, and F. W. Tavares, "Thermodynamic equilibrium in systems with multiple adsorbed and bulk phases," *Chem. Eng. Sci.*, vol. 60, no. 6, pp. 1773–1782, 2005.

[48] L. Michelsen, "The isothermal flash problem. part 1. stability," *Fluid phase Equilibra, Sci. Elsevier*, vol. 9, pp. 1–19, 1982.

[49] J. A. Nelder and R. Mead, “A simplex method for function minimization.pdf,” *Computer Journal*, vol. 7. pp. 308–313, 1965.

[50] J. W. Lee, H. C. Kang, W. G. Shim, C. Kim, and H. Moon, “Methane adsorption on multi-walled carbon nanotube at (303.15, 313.15, and 323.15) K,” *J. Chem. Eng. Data*, vol. 51, no. 3, pp. 963–967, 2006.

[51] Jr. T. D. McMinn, “Thesis, University of Texas.” Dortmund Data Bank Software & Separation Technology (DDBST), Version 2013, Texas, 1952.

[52] J. W. Lee, W. G. Shim, M. S. Yang, and H. Moon, “Adsorption isotherms of polar and nonpolar organic compounds on MCM-48 at (303.15, 313.15, and 323.15) K,” *J. Chem. Eng. Data*, vol. 49, no. 3, pp. 502–509, 2004.

[53] M. S. Sun, D. B. Shah, H. H. Xu, and O. Talu, “Adsorption equilibria of C 1 to C 4 alkanes , CO2 , and SF6 on silicalite,” *J. Phys. Chem. B*, vol. 102, no. 4, pp. 1466–1473, 1998.

[54] M. Thommes, R. Köhn, and M. Fröba, “Sorption and pore condensation behavior of pure fluids in mesoporous MCM-48 silica, MCM-41 silica, SBA-15 silica and controlled-pore glass at temperatures above and below the bulk triple point,” *Appl. Surf. Sci.*, vol. 196, no. 1–4, pp. 239–249, 2002.

[55] E. L. First, C. E. Gounaris, J. Wei, and C. A. Floudas, “ZEOMICS - Zeolites and Microporous Structures Characterization,” *http://helios.princeton.edu/zeomics/*, 2011. [Online]. Available: http://helios.princeton.edu/zeomics/. [Accessed: 30-

May-2016].

APPENDIX A

Peng-Robinson equation of state for confined fluids

Canonical partition function

$$Q(T,V,N_1,N_2,...,N_{NC}) = \prod_{i=1}^{NC}\left(\frac{q_{\text{int},i}^{N_i}}{\lambda_i^{3N_i} N_i!}\right) V_f^N \quad \exp\left(\int_{\infty}^{T}\frac{E_{conf}}{kT^2}\,dT\right)$$

Thermodynamic relations for the canonical partition function

$$P = kT\left(\frac{\partial \ln Q}{\partial V}\right)_{T,N_1,N_2,...,N_{NC}}$$

$$\mu_i = -kT\left(\frac{\partial \ln Q}{\partial N_i}\right)_{T,V,N_j\neq i}$$

Free volume

$$V_f = V - \sum_{i=1}^{NC}\frac{N_i}{\rho_{\max,i}}$$

$$\rho_{max,i}\sigma_i^3 = c_1 - c_2\exp\left(c_3\left(0.5-\frac{r_p}{\sigma_i}\right)\right) + c_4\exp\left(c_5\left(0.5-\frac{r_p}{\sigma_i}\right)\right)$$

$$\sigma_i = \sqrt[3]{\frac{c_1}{N_{av}}b_i}$$

with c_1 = 1.158, c_2 = 0.479, c_3 = 0.621, c_4 = 0.595, and c_5 = 4.014.

Configurational energy

$$E_{conf} = -\sum_{i=1}^{NC}\sum_{j=1}^{NC}\left(\frac{N_j}{2}N_{C,ij}\varepsilon_{ij}\right) - \sum_{i=i}^{NC}\left(N_i F_{p,i}\varepsilon_{p,i}\right)$$

Fraction of the fluid molecules in the confined space subjected to the attractive field of the pore walls

$$F_{p,i} = F_{pa,i} + (1 - F_{pa,i})\left(1 - \exp\left(-\frac{\varepsilon_{p,i}}{kT}\right)\right)\left(1 - \frac{x_i \rho}{\rho_{\max,i}}\right)^{\theta_i}$$

For random distribution of the fluid molecules inside the pore

$$F_{pa,i} = \frac{\left(r_p - \sigma_i / 2\right)^2 \left(r_p - \sigma_i / 2 - \delta_{p,i}\right)^2}{\left(r_p - \sigma_i / 2\right)^2}$$

Geometric term

$$\theta_i = \frac{r_p}{\delta_{p,i} + \sigma_i / 2}$$

Extended Peng-Robinson EOS for confined fluids:

$$P = \frac{RT}{v - b_p} - \frac{a_p(T)}{v\left(v + b_p\right) + b_p\left(v - b_p\right)} - \sum_{i=1}^{NC}\left(x_i \theta_i \frac{x_i b_{p,i}}{v^2}\left(1 - \frac{x_i b_{p,i}}{v}\right)^{\theta - 1}\left(1 - F_{pa,i}\right) \times \left(RT\left(1 - \exp\left(-\frac{N_{av}\varepsilon_{p,i}}{RT}\right)\right) - N_{av}\varepsilon_p\right)\right)$$

Confinement-modified energy parameter of fluid mixture:

$$a_p = \sum_{i=1}^{NC}\sum_{j=1}^{NC}\left(x_i x_j \sqrt{a_i a_j}\left(1 - \frac{2}{5}\frac{\sigma_{ij}}{r_p}\right)\right)$$

Confinement-modified volume parameter of fluid mixture:

$$b_p = \sum_{i=1}^{NC} x_i \left(\frac{N_{av}}{\rho_{\max,i}}\right)$$